JOURNAL OF GEOPHYSICAL RESEARCH, VOL. 105, NO. C9, PAGES 21,947–21,968, SEPTEMBER 15, 2000

Yellow and East China Seas response to winds and currents

G. A. Jacobs
Naval Research Laboratory, Stennis Space Center, Mississippi

H. B. Hur
Navy, Seoul, Republic of Korea

S. K. Riedlinger
Naval Research Laboratory, Stennis Space Center, Mississippi

Abstract. The influences of the Kuroshio Current (KUC), Taiwan Warm Current (TWC), and surface wind stress on the Yellow and East China Seas (YES) are examined using tracers in a Princeton Ocean Model. Two experiments are performed: one with wind stress and one without. Seasonal variations in the inflow and outflow of the TWC and Tsushima Current are specified to examine the effects of the current transports. Two separate tracers are inserted into each model experiment to track the pattern of KUC and TWC waters into the YES. The two main areas of KUC and TWC water movement into the Yellow Sea are the southern entrance to the Yellow Sea trough and the Yangtze Relict River valley. Results indicate that KUC and TWC waters advect into the Yellow Sea regardless of wind stress. However, in the Yellow Sea during winter the wind stress increases KUC and TWC concentration at 20 m. The wind stress also produces short time period events that horizontally advect water masses and spatially smooth seasonally averaged water mass concentrations. The bottom Ekman layer appears to be one of the mechanisms driving the northward bottom flow across the East China Sea shelf. The bottom friction layer is stronger in summer when the TWC velocity is high. The bottom friction layer draws KUC water across the bottom of the continental shelf into the Yangtze Relict River valley and generates upwelling along the Chinese coast.

1. Introduction

Two prominent theories of the Yellow and East China Seas (YES) circulation are provided by *Nitani* [1972] and *Beardsley et al.* [1985] (Figure 1). The main currents flowing into and out of the YES are the Kuroshio Current (KUC) flowing along the shelf break, the Taiwan Warm Current (TWC) entering through the Taiwan Strait, and the Tsushima Current (TSC) exiting through the Tsushima Strait. These external sources combine with local wind stress to force the ocean circulation and control the ocean environment in the YES. The KUC intrudes northeast of Taiwan onto the shelf mainly during winter when the TWC is weak [*Qiu and Imasato*, 1990; *Chern and Wang*, 1992; *Liu et al.*, 1992; *Hsueh et al.*, 1993; *Chuang and Liang*, 1994; *Su et al.*, 1994]. The TSC separates from the KUC near the shelf break [*Lie and Cho*, 1994; *Katoh et al.*, 1996], flows northward to the vicinity of Cheju Island, and exits the region through the Tsushima Strait.

One of the characteristic features of the Yellow Sea is the Yellow Sea Warm Current (YSWC) that flows beneath the surface northward from the area just west of Cheju Island [*Lie and Cho*, 1994]. The YSWC advects warm waters into the Yellow Sea that often produce surface effects observed in satellite sea surface temperature (SST), particularly during winter [*Zheng and Klemas*, 1982; *Chen et al.*, 1994]. Since the TSC flows northward from the Cheju Island area, the YSWC is often viewed as a branch from the TSC. Observations indicate that the YSWC is most apparent in winter and weak in summer [*Park*, 1986]. The warm saline water mass has been observed through in situ conductivity-temperature-depth (CTD) measurements [*Chen et al.*, 1994], and northward winter flow events have been related to wind stress and observed by current meters [*Hsueh*, 1988].

The KUC intrusions onto the continental shelf serve as the main source of warm saline water controlling the local environment [*Park*, 1986; *Guan*, 1994; *Lie and Cho*, 1994; *Su et al.*, 1994; *Su and Weng*, 1994]. In addition to the KUC, the TWC is a significant contributor to the water masses in the YES region [*Beardsley et al.*, 1985; *Fang et al.*, 1991; *Liu et al.*, 1992]. Prior research into the regional circulation has suggested quite different relative importances of the KUC and TWC to the YES environment (Figure 1). *Nitani* [1972] and others [*Lie*, 1986; *Park*, 1986; *Hu*, 1994; *Lie and Cho*, 1994] propose that the YSWC originates from the KUC (by means of the branching of the TSC) and then flows northward through the Yellow Sea trough. Other studies suggest that the YSWC originates from the inflow of the TWC across the East China Sea shelf [*Zheng and Klemas*, 1982; *Beardsley et al.*, 1985; *Chen et al.*, 1994]. There are additional studies that consider the water entering the Yellow Sea through the YSWC to be a mix of the TWC, KUC, and local East China Sea shelf waters [*Liu et al.*, 1992; *Su and Weng*, 1994]. The mechanism forcing intermittent northward

Paper number 2000JC900093.
0148-0227/00/2000JC900093$09.00

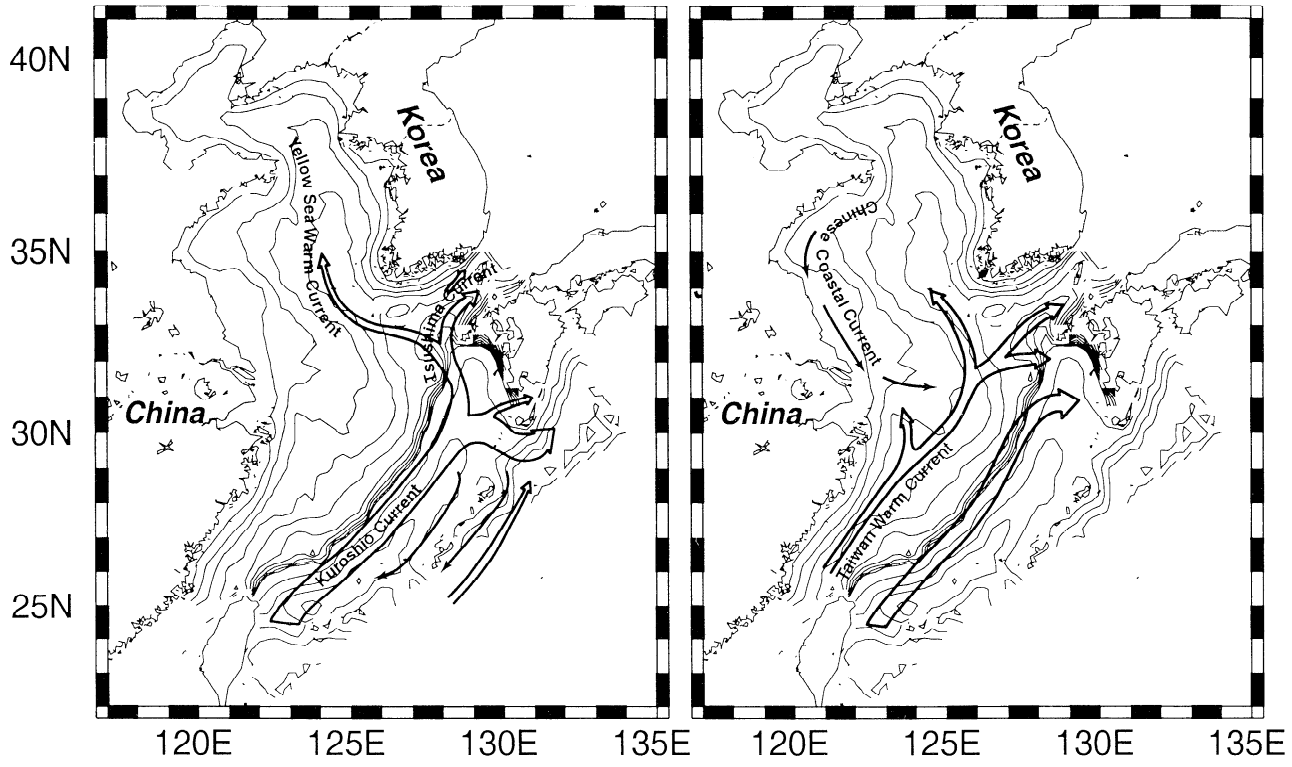

Figure 1. Results from prior investigations into the Yellow and East China Seas circulation indicate the difficulty in determining the importance of different water mass sources purely from observations. Results adapted from *Nitani* [1972] (left) suggest the Kuroshio Current as the main source for the Yellow Sea Warm Current, while results adapted from *Beardsley et al.* [1985] (right) suggest the Taiwan Warm Current as the main source with an additional intrusion into the Yangtze Relict River valley.

flow into the Yellow Sea has been suggested by *Hsueh* [1988] to be the winter northerly wind bursts. The northerly wind bursts push surface waters southward by means of the Chinese and Korean Coastal Currents and set up a northward pressure force that drives the subsurface flow into the Yellow Sea [*Hsueh*, 1988; S. K. Riedlinger and G. A. Jacobs, A study of the dynamics of wind-driven transports into the Yellow Sea, accepted to *Journal of Geophysical Research*, 2000, hereinafter referred to as Riedlinger and Jacobs, accepted manuscript, 2000.]. Additional studies suggest the importance of the bottom Ekman boundary layer in producing upwelling along the Chinese coast [*Hu*, 1994].

To add to the previous studies, we attempt to understand the importance of the KUC and TWC transports and the local wind stress to the YES environment from the point of view of numerical model tracer experiments. Numerical models provide one source to separate and understand the importance of different dynamical mechanisms as well as to understand the importance of the currents and local wind stress in generating the YES environment. Thus the numerical model provides a controlled test environment that is not possible in the true ocean.

The velocity structure provides an understanding of the general circulation and processes that control water mass formation. We use the velocity field in addition to salinity fluxes to examine the YES circulation in section 3. However, the model velocity field does not always provide an objective direct indication of flow pathways and the formation of water masses. When subjectively interpreting a presentation of the velocity field, the actual fluid particle trajectory is not well determined. The boundary of water from two origins, such as the boundary between the KUC and TWC at the shelf break, is not always well defined by the velocity field. The currents do not indicate the effects of important processes such as vertical and horizontal turbulent mixing. Time-averaged velocities also do not portray the effects due to short time period transport variations. To complement the model velocity distribution, the pathways of KUC and TWC transport are examined by adding tracers to the numerical model. The tracers behave as conservative quantities subjected to the prescribed ocean dynamics.

In addition to objectively marking the paths taken by water originating from the tracer insertion points, the tracer experiment may be designed to provide additional information. Separate tracers are added to the TWC and KUC so that the path of each may be examined in isolation. The tracers then provide an estimate of the individual KUC and TWC flow patterns into the Yellow Sea. To examine vertical motions, we set the tracer concentration at the inflow equal to the depth. Thus, at a particular depth, if a tracer concentration is greater than the depth, it will be due to water's having upwelled to the new depth. This may occur through local upwelling, upwelled water advecting, or upward vertical mixing. Several processes may decrease the tracer concentration, such as horizontal and vertical mixing in addition to downwelling.

The effects of inflow variations are examined through the seasonal cycle. The TWC and TSC transports are specified with seasonal variations. By examining the differences between the seasonal tracer distributions, some insight is provided into the effects of variations in the currents. Finally, we also examine the

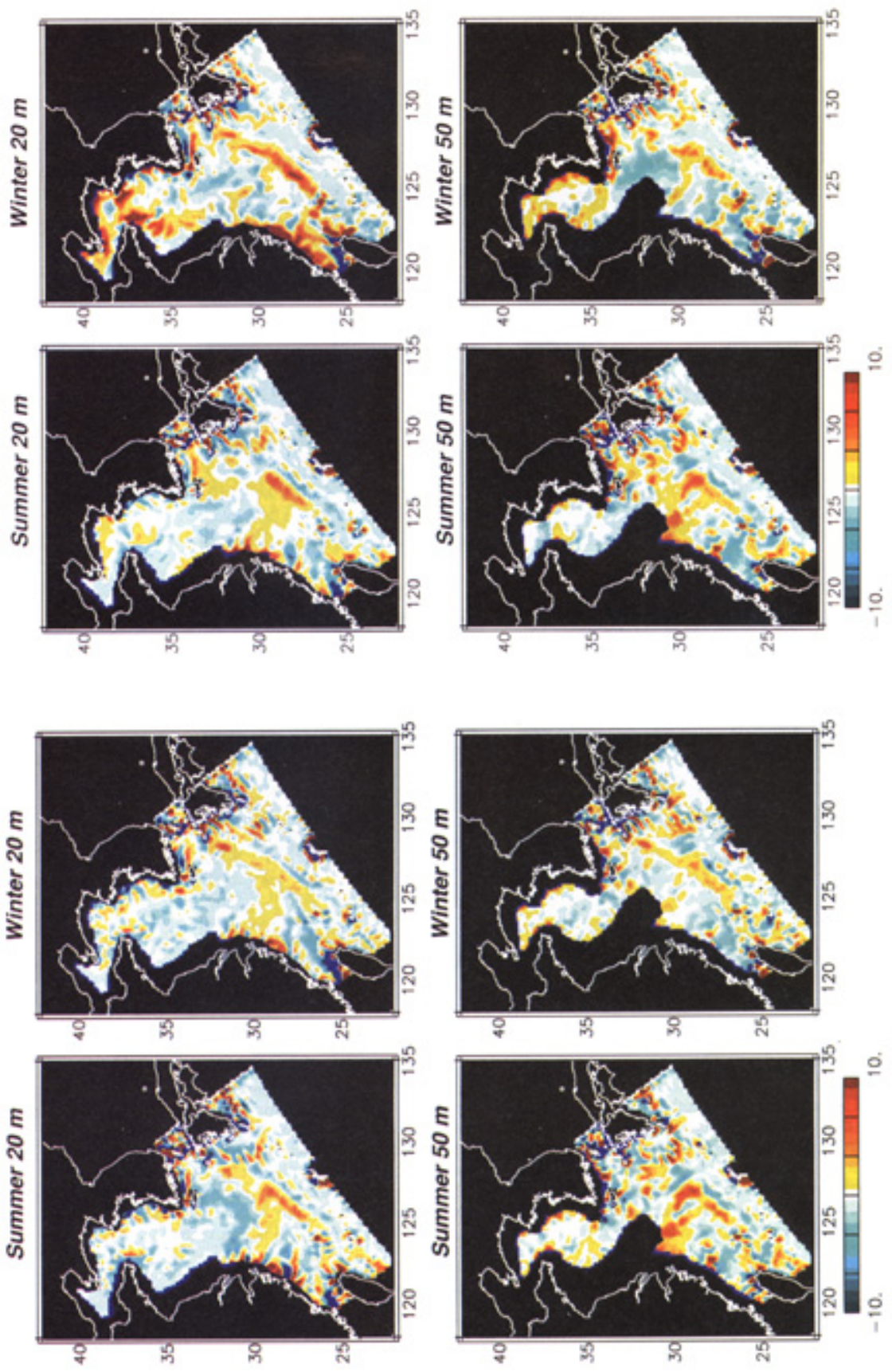

Plate 1. The salinity fluxes in the model experiment without wind indicate salt inflow across the shelf break, influx through the area along the Korean coast, increased salinity fluxes into the Yangtze Relict River valley during summer, and much less inflow to the Yellow Sea than the experiment with wind stress (Plate 2). The color bar units are 10^{-7} practical salinity units (psu) s^{-1}.

Plate 2. The salinity fluxes in the model experiment with wind indicate salt inflow across the shelf break, through the area southeast of Cheju Island, increased salinity flux into the Yangtze Relict River valley during summer, and increased salt inflow to the Yellow Sea during winter. The color bar units are 10^{-7} psu s^{-1}.

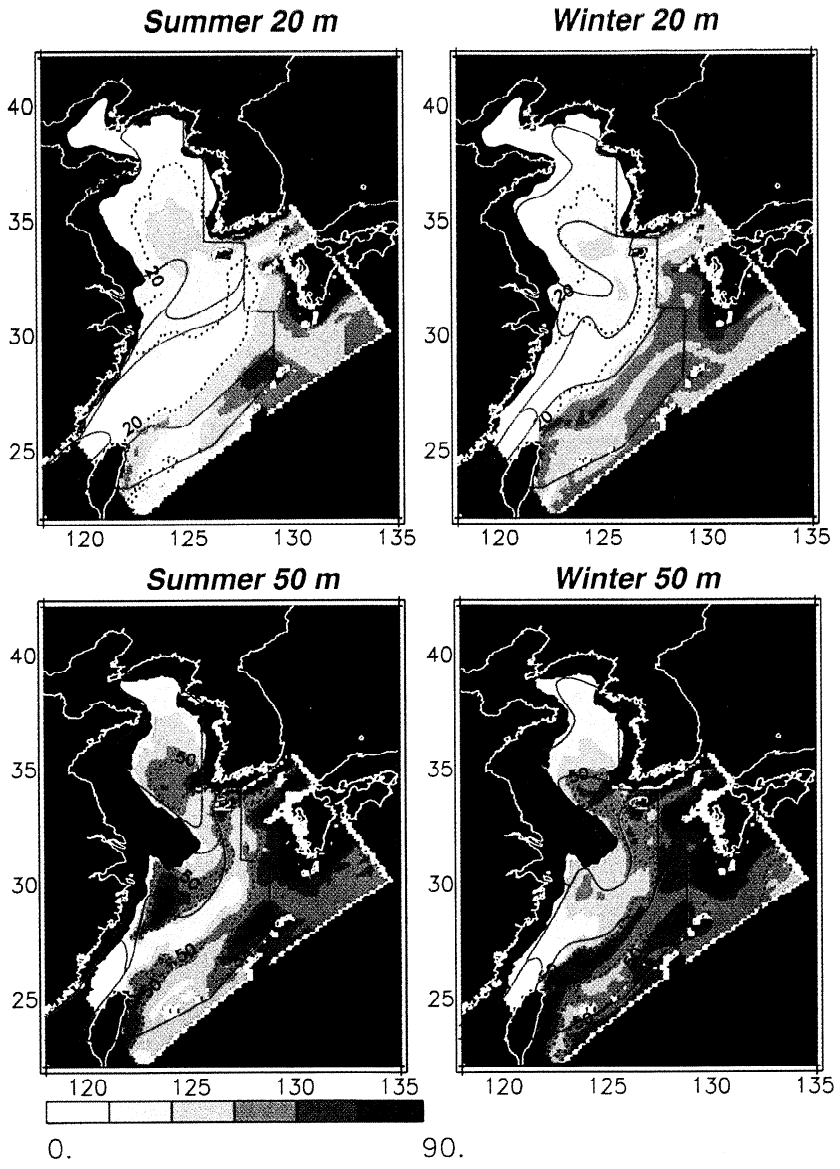

Plate 3. In the model experiment without wind forcing the Kuroshio Current tracer concentration at the boundary is specified to be equal to the depth. Thus concentration values greater than the depth indicate water originating from lower depths. Because wind forcing is excluded, the differences between summer and winter are caused by variations in the Taiwan Warm Current and Tsushima Current transports. In the without-wind experiment the Kuroshio flows into the Yellow Sea and Yangtze Relict River valley. The five outlined areas are surface and bottom water mass distributions (adapted from *Liu et al.*, [1992]). The KUC is the southernmost area, the TWC is in the Taiwan Strait, the East China Sea Water extends from the Taiwan Strait, the Yellow Sea Water is the northernmost area, and a mixed water mass lies between the Yellow Sea and East China Sea Waters.

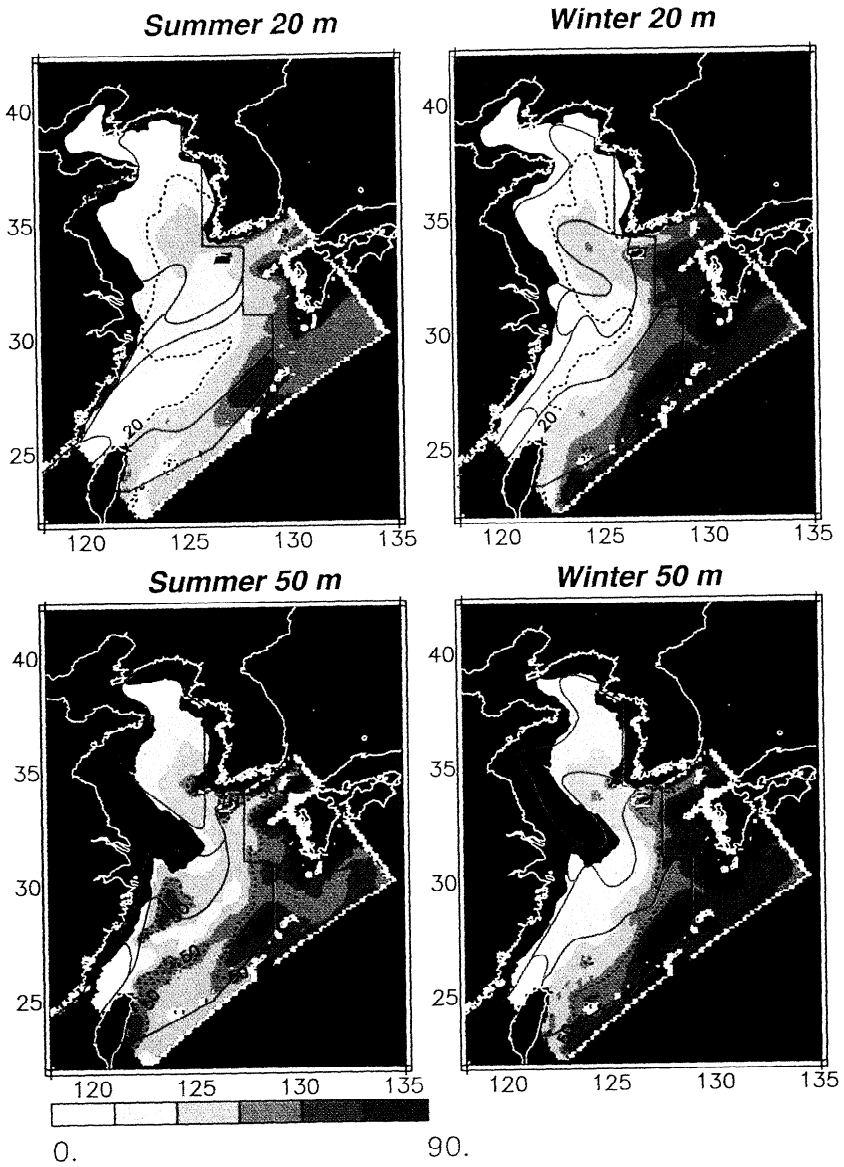

Plate 4. In the model experiment with wind forcing the Kuroshio Current tracer concentration at the boundary is specified to be equal to the depth. Concentration values greater than the depth indicate water originating from lower depths. The wind forcing causes the concentrations to be spatially smoother than the model without wind forcing. The 50 m winter intrusion into the Yangtze Relict River valley is reduced, and the 20 m winter intrusion into the Yellow Sea trough is increased. The five outlined areas are surface and bottom water mass distributions (adapted from *Liu et al.*, [1992]). The KUC is the southernmost area, the TWC is in the Taiwan Strait, the East China Sea Water extends from the Taiwan Strait, the Yellow Sea Water is the northernmost area, and a mixed water mass lies between the Yellow Sea and East China Sea waters.

effect of local wind stress by performing two model experiments. Each experiment contains seasonally varying current transports and the KUC and TWC tracers with depth-varying inflow concentration. However, the first experiment does not contain the effects of the surface wind stress, while the second experiment does.

The model is described in more detail (section 2), and resulting summer and winter current and salinity flux fields are then examined (section 3). Tracers are added to the model, and the flow into the Yangtze Relict River valley and Yellow Sea trough are examined (section 4). Tracer variations along three transects are examined (section 5). Several different dynamical mechanisms are at work, and each mechanism is dominant in differing areas.

2. The Model

In this study we use a numerical dynamic/thermodynamic model of the Yellow and East China Seas based on the Princeton Ocean Model [*Blumberg and Mellor*, 1987] with an enhanced vertical turbulence closure scheme [*Kantha and Clayson*, 1994]. The model region (Figure 2) includes the Bohai Bay, Yellow Sea, and East China Sea with an extension into the deep Pacific to allow inflow and outflow of the Kuroshio Current system. The model uses a rectilinear horizontal grid with variable spacing from 25 to 8 km, and the model grid is rotated 39° from true north (Figure 2). There are 24 sigma levels vertically to a maximum allowed depth of 2000 m. Bottom topography for the model and identification of major regional features is shown in Figure 3.

The southeastern model boundary (south of the Ryukyu Islands) is closed to transport. The Taiwan Strait, Tsushima Strait, and the Kuroshio south of Taiwan and Japan are open boundaries. The Kuroshio inflow temperature and salinity vary seasonally, and the temperature and salinity distributions across the Kuroshio inflow boundary are taken from *Nitani* [1972]. The temperature and salinity determine geostrophic velocities using a depth of no motion at 600 m. From the geostrophic velocity the annual average transport is applied at the four model grid points south of Taiwan. Thus the inflow width of the Kuroshio is set to about 100 km, and the resulting horizontal distribution across the stream is roughly parabolic with vertical distribution decreasing to 0 at and below 600 m. The total transport computed from the inflow velocity is scaled to 23 Sv. Kuroshio outflow boundary conditions are computed in a similar manner. The total outflow Kuroshio transport is set to 22 Sv [*Zhao and Fang*, 1991]. The outflow temperature and salinity are derived from advection boundary conditions. Thus the value at the boundary is determined by the temperature and salinity advected to the boundary from the interior.

The TWC inflow temperature and salinity are determined from historical average profiles in the National Oceanographic Data Center database. The inflow temperature and salinity values vary seasonally. The TWC is mainly barotropic, and the velocity distribution across the strait and with depth is set to a uniform current. The total transport through the strait is set to 0.6 Sv in winter, 1.3 Sv in spring, 2.5 Sv in summer, and 1.1 Sv in fall [*Fang et al.*, 1991]. Transports are interpolated linearly in time to the model time. The transport through the Tsushima Strait is set to be 1.0 Sv higher than the TWC inflow [*Fang et al.*, 1991]. The Tsushima outflow distribution is vertically constant with the east and west branches of the TSC each covering four model grid points with a roughly parabolic distribution and having equal transport. The outflow conditions

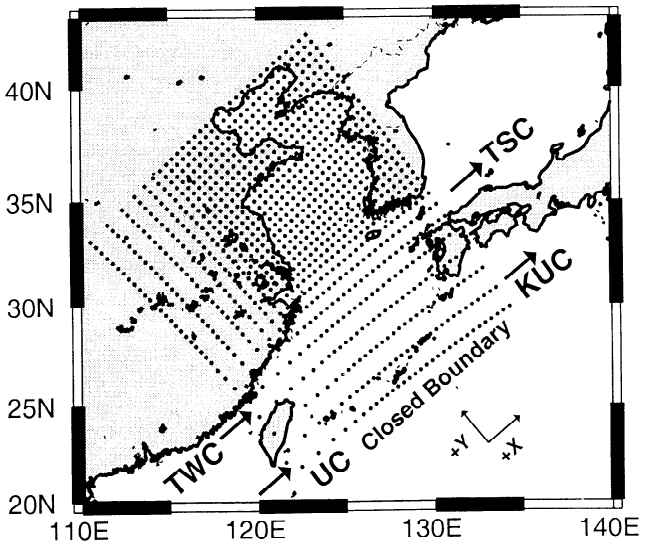

Figure 2. The model is defined on a telescoping grid with 25 km resolution in the East China Sea and decreasing to 8 km resolution in the northern Yellow Sea. The grid displayed here is every fifth point. The Kuroshio Current (KUC) is prescribed as a constant transport, and the Taiwan Warm Current (TWC) and Tsushima Current (TSC) transports vary seasonally. The southeastern boundary is closed to transport. Inflow temperature and salinity vary seasonally.

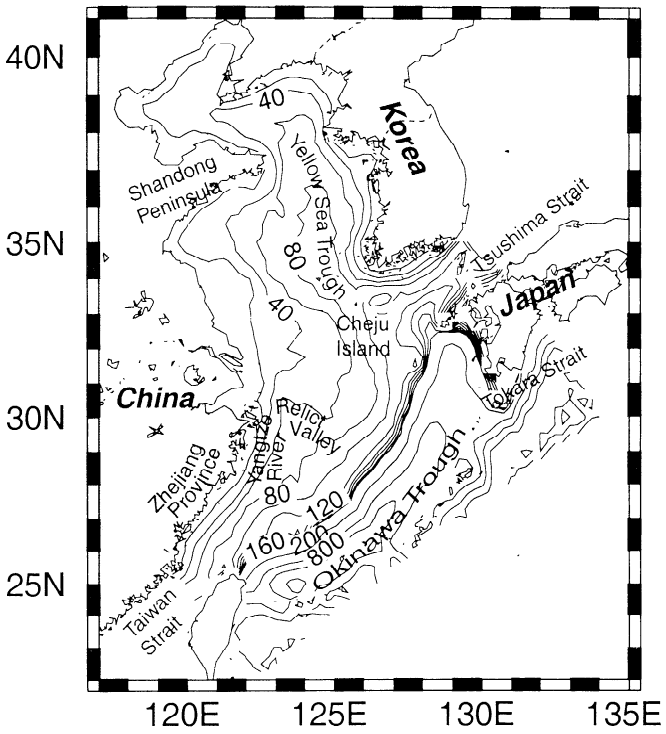

Figure 3. The Yellow and East China Seas bottom topography used in the numerical model contains the main Yellow Sea trough and the Yangtze Relict River valley southeast of the Yangtze River mouth.

for temperature and salinity are determined by advective boundary conditions.

For this study, no tidal elevations or tidal transports are applied at the boundaries. Previous studies have suggested the importance of tide-induced vertical mixing in generating the colder coastal water during summer [*Lie*, 1986; Zhao, 1989; *Wan et al.*, 1990; *Yang*, 1990]. It is important to understand the individual effects before combining the forcing sources, so we do not include the boundary tide forcing and tide potential in these model experiments.

Atmospheric forcing for 1993 through 1997 is from the Navy Operational Global Atmospheric Prediction System (NOGAPS) [Hogan *and Rosmond*, 1991; *Rosmond*, 1992; *Hogan and Brody*, 1993]. The NOGAPS data horizontal resolution is 1.25° x 1.25° with one value per day. All forcing and boundary inputs are linearly interpolated to the model time step. The model is initialized with the three-dimensional January climatological temperature and salinity developed at the Naval Oceanographic Office. Surface elevations and velocities are initially zero. The model simulations are run for 1 year with boundary forcing before tracers are added. The with-wind experiment has NOGAPS wind forcing applied during the 1-year spin up, while the without-wind experiment is not forced with surface wind stress during spin up. The model experiments are integrated another 6 months after setting boundary tracer concentrations before the results are examined. Thus a total of 1.5 years of spin up is run before data are extracted. The model results examined here are from 1995 through 1997.

Previous studies using this model have indicated its capability of generating the short time period variations associated with wind stress through comparison of satellite-observed sea elevation, in situ pressure gauge data, and model sea level elevation [*Jacobs et al.*, 1998a]. For the strongest wind events the model sea level peak anomalies are not as large as the observed. This may be due to the NOGAPS wind stress's not containing sufficiently strong winds. In response to wind events, continental shelf waves are generated and propagate southward from the Bohai Bay along the Chinese coast [*Jacobs et. al.*, 1998b]. These waves are observed in both the satellite data and the model results, and the results agree favorably in terms of amplitude, phase speed, and wavelength.

In order to examine the spatial coverage of the inflowing currents, tracers are added to the numerical model. The dynamics affecting the tracer concentrations are identical to the dynamics determining the temperature or salinity in the model. Thus the tracers are affected by the advection as well as the horizontal diffusion prescribed by the Smagorinsky diffusion scheme and the vertical diffusion prescribed by the turbulence closure described by *Kantha and Clayson* [1994]. No surface or bottom forcing of the concentration is applied. Tracer concentrations are specified at the KUC and TWC inflow ports. Separate fields are used for the two tracers so that the tracer concentrations do not interact with or affect one another. The concentration is set to a value equal to the depth, and the horizontal distributions of tracer concentrations are constant across each respective inflow port. The outflow tracer boundary condition is an advection condition. Thus the outflow boundary value is determined by the upstream concentration.

3. Velocity, Salinity Flux, and Bottom Current Distributions

It is not possible to present the entire three dimensional (3-D) velocity field and its seasonal variations. To aid in distilling and

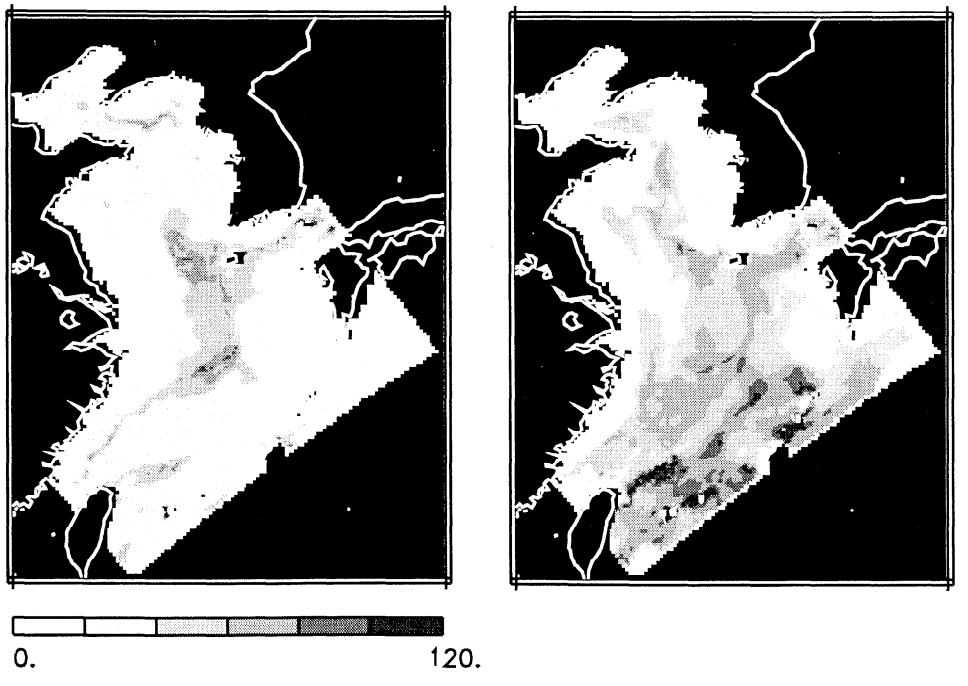

Figure 4. The depth of the mixed layer during (left) summer and (right) winter is mainly controlled by strong northerly winds during winter. The northerly winds increase vertical mixing and deepen the mixed layer. The mixed layer here is defined as the depth at which the temperature is 0.2°C less than the surface temperature. The mixed layer depth is generally below 20 m throughout the year. Thus we examine variations at the 20 and 50 m depths throughout this paper.

concentrating the results, we present quantities at two depths and only in summer and winter. On the basis of climatological water mass studies [*Hur et al.*, 1999], seasons are separated as winter (January through March), spring (April through June), summer (July through September), and fall (October through December). Seasonal averages presented here are based on the 3 years of model output after the initial spin up to minimize the effects of interannual and intra-annual variations. To determine the depths that would be most illuminating, we first examine the mixed layer depth from the model experiment with wind forcing (Figure 4). We use a simple definition to calculate the mixed layer depth, which is the depth at which the temperature is 0.2°C colder than the local surface water. In general, the winter mixed layer depths are greater than the summer depths as would be expected because of the stronger vertical mixing induced by increased winter wind stress. The mixed layer depth is generally 20 m or greater throughout most of the Yellow Sea during both summer and winter. Previous examinations of thermocline depth [*Dianrong et al.*, 1990; *Zhao*, 1989] indicate favorable agreement with these results.

For depths to examine we would like to choose a depth above and a depth below the mixed layer since the Yellow Sea is dominated by a strong thermocline during summer. We choose 50 m as a depth below the thermocline. The summer mixed layer depth in the area of Cheju Island is >50 m at several points (Figure 4). Thus the 50 m depth is not entirely out of the influence of the mixed layer in this area. A depth >50 m would not be as revealing since it would not cover much of the Yellow Sea area. One opposing factor in choosing a depth above the thermocline is the influence of wind forcing. The surface is strongly influenced by the direct momentum transfer of wind stress and by the Ekman balance. We wish to remain as far as possible from the surface to assess the effects of the wind stress on circulation below the Ekman layer. We choose 20 m as the upper layer depth since this is far from the surface, above the mixed layer depth (though only slightly so in summer), and generally, regarded as at the YSWC depth.

3.1. Velocity Fields

Local wind stress is one of the principal forcing mechanisms within this region. To understand the impact of wind stress, we first examine the model velocities without the effect of wind stress. This velocity field is the result of the prescribed open boundary conditions and the thermohaline forced circulation. The effects of wind stress are demonstrated by differencing the velocity fields of the model with wind stress applied and the velocity fields without wind stress applied. Both without and with wind stress the YSWC flows northward into the Yellow Sea, and the Chinese and Korean Coastal Currents flow southward. However, the physical mechanisms connecting the coastal currents and the YSWC differ between the with and without wind stress situations.

Without wind stress applied the summer and winter mean currents at 20 and 50 m (Figure 5) indicate many of the observed circulation features. The KUC and TWC flows across the East China Sea are apparent along with the seasonal variations in the TWC flow. At 20 m the Chinese Coastal Current flows southward around the tip of the Shandong peninsula and along the Chinese coast. The Chinese Coastal Current flows south only to a point north of the Yangtze River mouth rather than along the entire Chinese coast to the Taiwan Strait as observed [*Zheng and Klemas*, 1982; *Guan*, 1994]. The Chinese Coastal Current without wind stress is stronger in summer. A southward flow along the Korean peninsula forms the Korean Coastal Current [*Zheng and Klemas*, 1982]. The Korean Coastal Current appears at both 20 and 50 m in summer and winter.

The TSC appears to separate from the KUC near 127°E, flow northward, and split, with a portion turning northeastward south of Chuju Island and a portion turning northwestward southwest of Cheju Island. The TSC separation from the KUC is consistent with that observed by *Lie et al.* [1998]. The northwestward flow into the Yellow Sea from the area southwest of Cheju Island may be identified as the YSWC. A portion of the northwest flow enters the Cheju Strait by turning its direction clockwise, and this clockwise turning flow is named the Cheju Warm Current by *Lie et al.* [1998]. At 20 m most of the flow turns to the east, north of Cheju Island, and exits the Yellow Sea, and only a small portion flows northward into the YSWC. At 50 m much more of the flow forms into the YSWC, with stronger northward flow during summer.

Since the results are from the model without wind forcing, wind forcing is not the sole forcing of the YSWC branching from the TSC and flowing into the Yellow Sea. The southward flowing Chinese and Korean Coastal Currents are a mass balance response to the northward flowing YSWC. In addition, the YSWC appears stronger in summer than in winter without wind forcing, and this situation is opposite to that observed.

The strength of flow into the Yangtze Relict River valley contains strong seasonal variation. Flow into the valley is generally northward, with reduced strength in winter. This flow is related to the TWC strength. The higher TWC transport during summer leads to a much larger intrusion than during winter. This is also true for the TSC, though the TSC does not indicate variations as large. Without wind stress, northward flow occurs into both the Yangtze Relict River valley and the Yellow Sea trough. One possible contributing factor is the bottom Ekman layer examined in section 3.3.

The effect of the wind stress on circulation is presented by differencing the seasonal means of the model experiments with wind stress and without wind stress (Figure 6). As the summer southerly monsoon winds generally have small amplitude, the summer circulation difference is small. At 20 m the Korean Coastal Current indicates a decrease in strength with wind stress (northward transport change). Also at 20 m the Chinese Coastal Current indicates a decreased strength north of the Yangtze River mouth (northward transport change) and increased strength (southward transport change) south of the Yangtze River mouth. The TSC south of Cheju Island indicates a slight decreased strength. At 50 m the summer wind stress generates a small increase in southward flow. One explanation for the decreased flow into the Yellow Sea is the sea level increase in the northern areas due to the southeasterly summer monsoon winds. The increased sea level provides a pressure gradient to prevent northward flow into the Yellow Sea.

The winter northwesterly monsoon wind stress magnitude is much larger than the summer monsoon wind stress, and thus the circulation effects are larger. At 20 m both the Chinese and the Korean Coastal Currents indicate large increases in southward flow relative to the no-wind experiment (Figure 6). Without wind stress the Chinese Coastal Current flow is weakly southward, with an area of northward flow occurring off the Yangtze River mouth. With wind stress the southward flow is much stronger, and no northward flow occurs along the Chinese

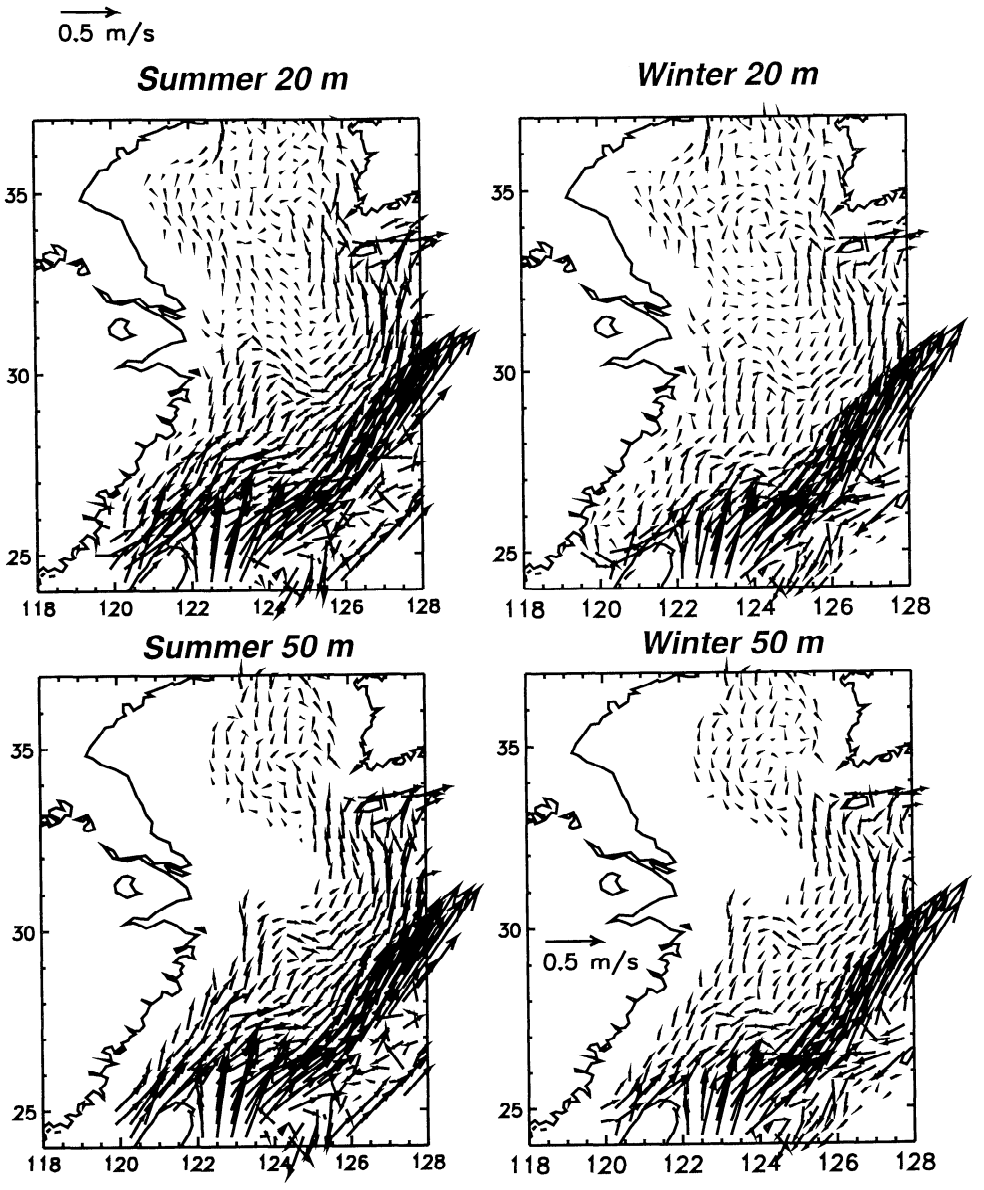

Figure 5. The mean velocity of the model without wind forcing indicates a northward flow west of Cheju Island, and southward Chinese Coastal Current north of the Yangtze River mouth, and a current into the Yangtze Relict River valley during summer and winter.

coast. The southward flow extends from the Shandong peninsula to the Taiwan Strait, which is the normally observed winter situation [*Zheng and Klemas,* 1982; *Su and Weng*, 1994]. The wind stress has the largest direct forcing effects in the shallowest areas. That is, the currents are in the direction of wind stress along the Chinese and Korean coasts where the surface and bottom boundary layers are not separate.

The increased southward coastal flow has been shown to decrease the sea level elevation in the northern Yellow Sea (*Riedlinger and Jacobs*, accepted manuscript, 2000). The northward pressure force accelerates the subsurface flow into the Yellow Sea [*Hsueh*, 1988]. The YSWC flow from west of Cheju Island increases at 20 and 50 m with wind stress. Wind forcing extends the YSWC into the Yellow Sea during winter as the northward flow in the Yellow Sea trough (Figure 6). Thus the YSWC leading from Cheju Island northward is strengthened by the northwesterly winter monsoon winds.

The winter flow into the Yangtze Relict River valley at 20 and 50 m decreases with the wind stress. The winter northerly wind stress pushes the surface water southward, and this increases the southward Chinese Coastal Current. The area covered by the southward flow extends an appreciable distance from the coast and down to 50 m. The deep southward flow reduces the northward flow into the Yangtze Relict River valley during winter.

From the velocity distributions, without wind forcing the YSWC flows into the Yellow Sea and the coastal currents are then forced southward. With wind stress the northerly winter winds drive the coastal currents more strongly southward, and the northward YSWC flows from the TSC. The difference between the two forcing situations is the pressure gradients through the region. Without wind stress the northward flowing YSWC generates a setup in the northern regions, and the subsequent pressure gradient drives the coastal flows southward. With wind stress the southward flowing coastal currents produce a setdown in the northern regions, and the YSWC is

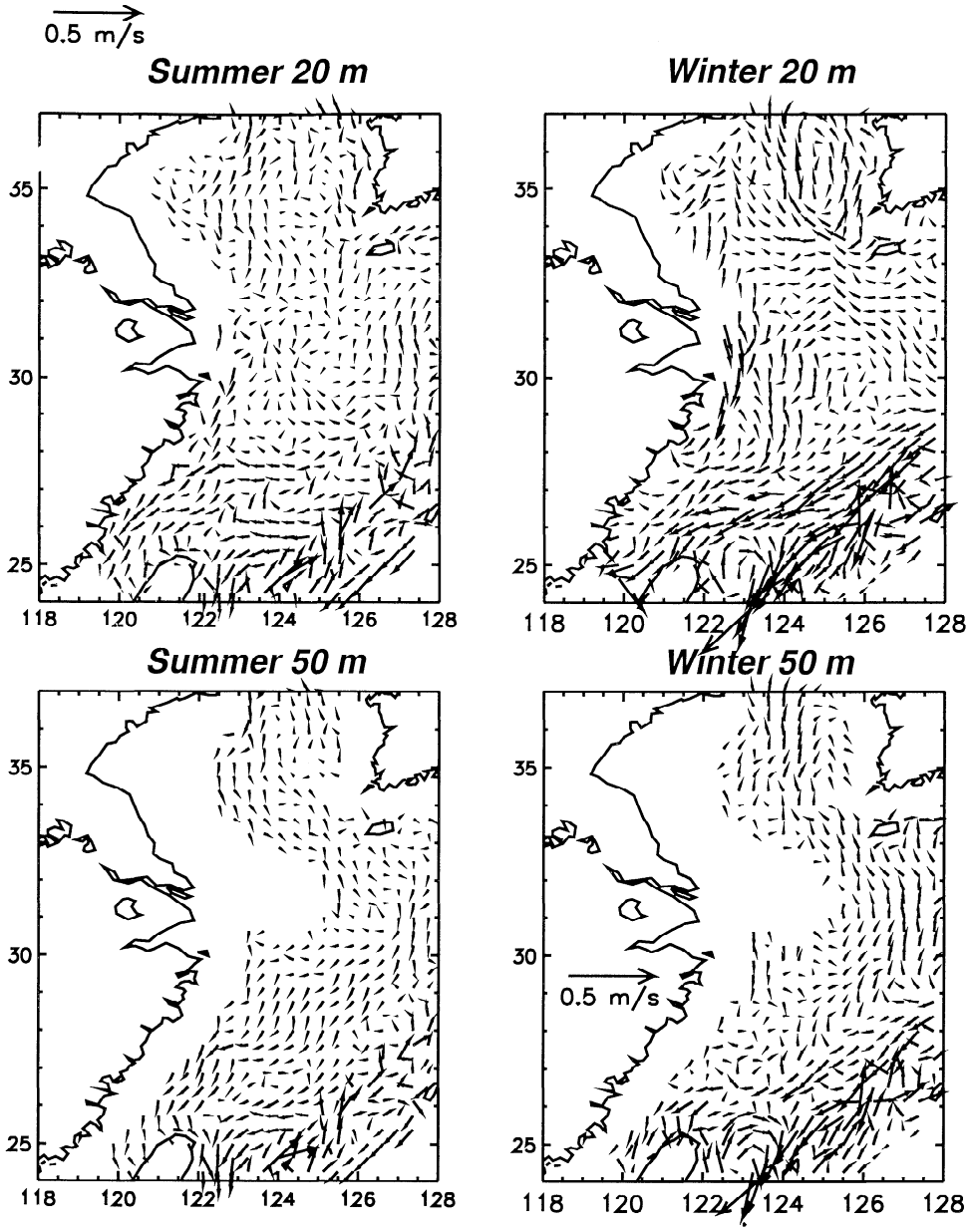

Figure 6. The velocity difference of the with-wind minus the without-wind experiments exemplifies the winter increase in the Chinese and Korean Coastal Currents, increased winter northward flow into the Yellow Sea just west of Cheju Island, and southward winter flow induced over the Yangtze Relict River valley. There is little difference between the with- and without-wind experiments during summer as the winds are generally weak during this time.

forced by the pressure gradient. The YSWC with wind forcing is stronger in the winter; thus the wind forcing brings the model YSWC seasonal variations in better agreement with observations

3.2. Salt Flux

The advective salinity flux is that portion due only to the horizontal advection component

$$-u\frac{\partial S}{\partial x}-v\frac{\partial S}{\partial y}.$$

The model contains a much more complete calculation of the salt flux, but we only examine the portion due to horizontal advection here. That is, fluxes due to horizontal and vertical mixing as well as to vertical advection are disregarded in this analysis. This is a measure of the transport of salt by the horizontal motions of currents and provides an indication of the areas of significant water mass formation or interaction. Note that the sign on the flux implies that a positive flux results in an increasing salinity. Model salinity fluxes without wind stress (Plate 1) indicate consistency between summer and winter with similar spatial patterns. The most prominent feature is the salt influx across the shelf break stretching from 125° to 128°E. This is an indication of saline KUC intrusion across the shelf as observed by *Chern and Wang* [1992] and *Zheng and Huang* [1993]. The model boundary conditions specify that 1 Sv of the KUC flows out through the Tsushima Strait. Thus this flux across the shelf break is largely controlled by the boundary conditions. Also contributing to the flux across the shelf break

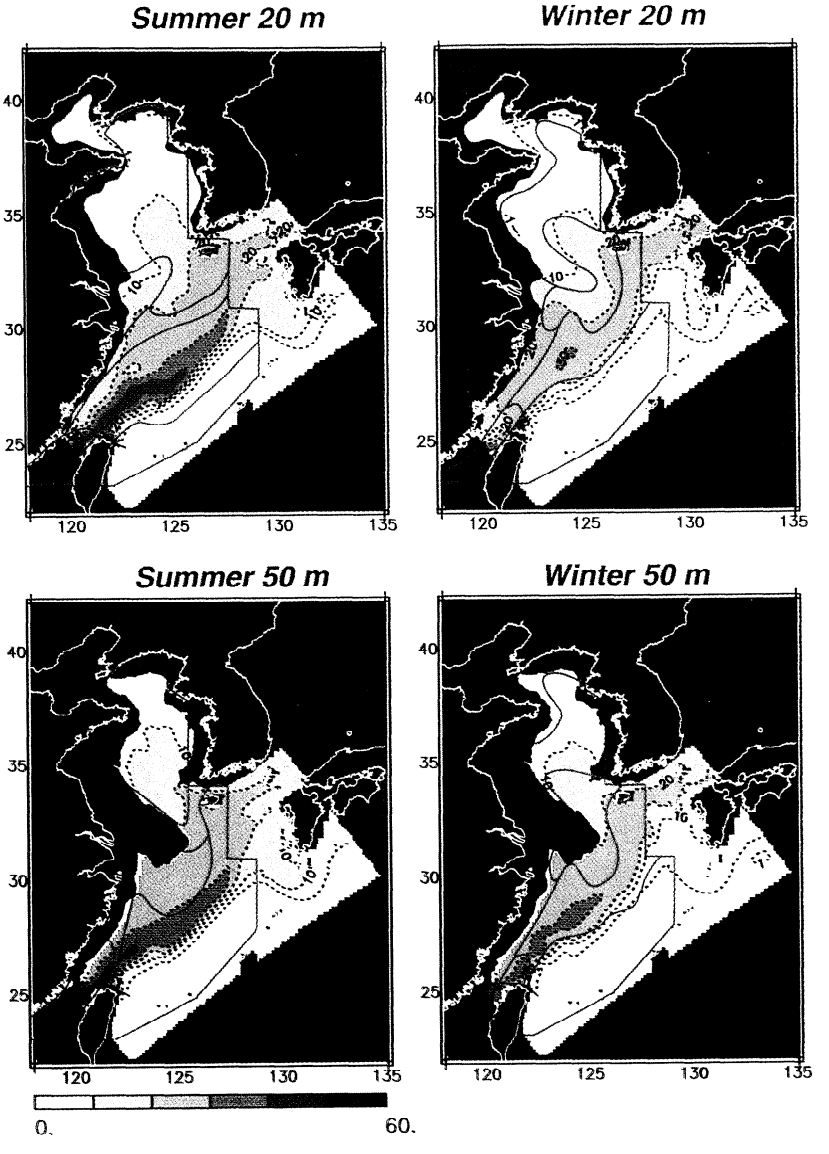

Plate 5. In the model experiment without wind forcing the Taiwan Warm Current tracer concentration at the boundary is specified to be equal to the depth. Concentration values greater than the depth indicate water originating from lower depths. A portion of the Taiwan Warm Current intrudes into the Yellow Sea trough and the Yangtze Relict River valley. The concentrations do not significantly decrease during winter when the Taiwan Warm Current transport is low, indicating that horizontal mixing is not large. The five outlined areas are surface and bottom water mass distributions (adapted from *Liu et al.*, [1992]). The KUC is the southernmost area, the TWC is in the Taiwan Strait, the East China Sea Water extends from the Taiwan Strait, the Yellow Sea Water is the northernmost area, and a mixed water mass lies between the Yellow Sea and East China Sea Waters.

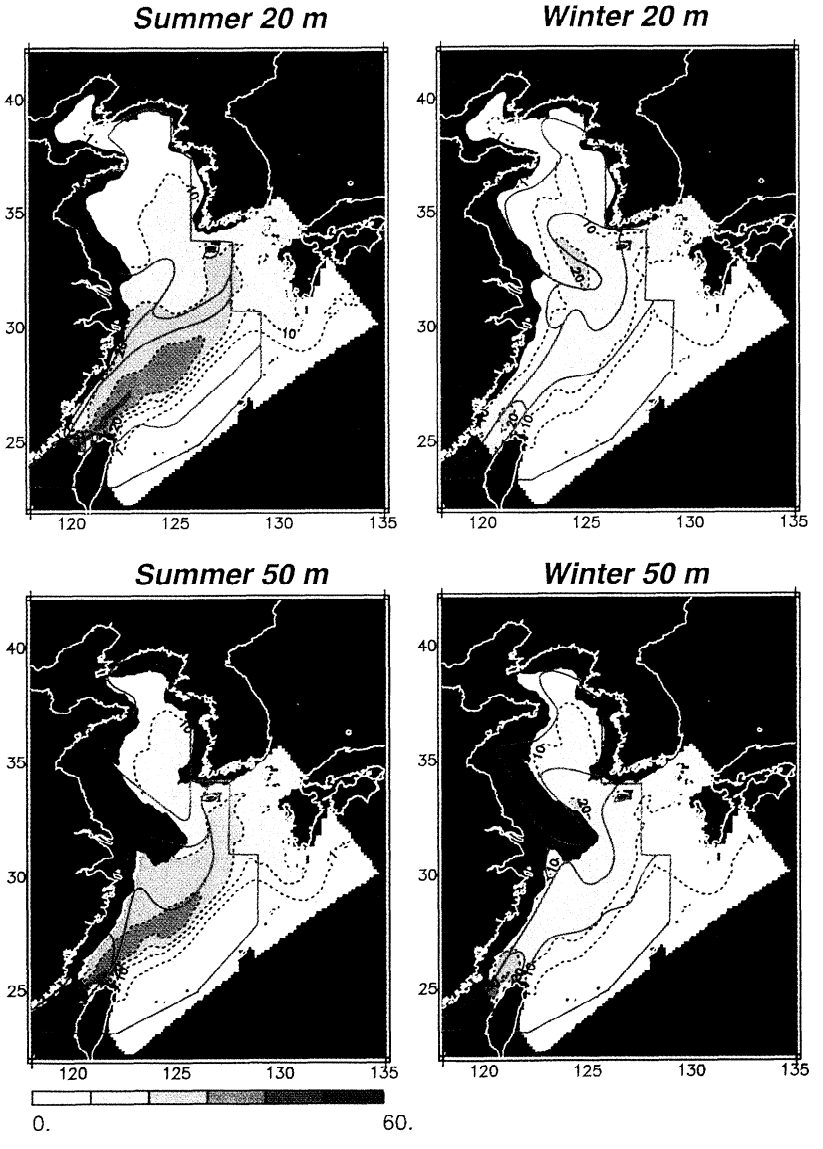

Plate 6. In the model experiment with wind forcing the Taiwan Warm Current tracer concentration at the boundary is specified to be equal to the depth. Concentration values greater than the depth indicate water originating from lower depths. During winter the extent of intrusion into the Yellow Sea trough is increased relative to the experiment without wind forcing. Also, the winter concentrations are much reduced due to increased horizontal mixing induced by the wind stress. The five outlined areas are surface and bottom water mass distributions (adapted from *Liu et al.*, [1992]). The KUC is the southernmost area, the TWC is in the Taiwan Strait, the East China Sea Water extends from the Taiwan Strait, the Yellow Sea Water is the northernmost area, and a mixed water mass lies between the Yellow Sea and East China Sea waters.

are intrusions from the KUC onto the shelf. Examination of the tracer concentrations in sections 4 and 5 indicate short time period intrusions of KUC water into the region normally covered by the TWC water. Observations of cold saline eddies and finger-like KUC intrusions have been made by *Chern and Wang* [1992] and *Hsueh et al.* [1993].

In addition to the KUC intrusion onto the shelf, the Yangtze Relict River valley indicates a relatively large salt influx that is highest at 50 m during summer. The fresh water outflow from the Yangtze River presents a strong horizontal salinity gradient, and the generally northward flow in the Yangtze Relict River Valley (Figure 5) would bring the saline TWC and KUC waters across this high gradient. The bottom boundary layer discussed in section 3.3 also aids in bringing Kuroshio water northward along the bottom of the shelf, and this mechanism may also contribute to the high salt flux at 50 m. When wind stress is applied to the model, the salt flux changes, most dramatically in the winter (Plate 2). The increased YSWC northward intrusion under the influence of wind stress would be expected to advect more saline KUC water into the Yellow Sea trough. The areas of high salt flux caused by this saline intrusion would be across the strongest salinity gradients. The largest salt flux areas at 20 m in winter with wind stress (Plate 2) occur to the north and west of the YSWC intrusion; that is, the high salt fluxes exist along an arc from the area east of Shandong peninsula southwestward to a line ~300 km off the China coast.

3.3. Bottom Boundary Layer

Hu [1994] proposes the bottom boundary layer Ekman transport as a possible mechanism for producing observed upwelling along the Chinese coast. The positive salinity flux in the Yangtze Relict River valley (Plate 1) is possibly due to bottom Ekman transport. To examine the bottom boundary transport, we average velocities over the bottom 5 m (bottom velocities) and compare them to the velocities averaged over the total depth (total velocities) in the model with wind stress applied (Figure 7). The bottom velocity is small where the depth is >200 m.

The largest bottom velocities occur on the shelf during summer when the TWC is strong (Figure 7a). In general, comparison of the bottom velocities to the total velocities indicates that the bottom velocities are turned to the left of the direction of the total velocities. This situation is expected in the bottom Ekman layer. In the Yangtze Relict River valley, where the total velocity generally follows the isobaths directed to the northeast, the bottom velocity indicates a northward transport across isobaths. In the TSC area south of Cheju Island, bottom velocities indicate a northwestward transport into the Yellow Sea, whereas the total velocity of the TSC is directed northward. The bottom velocities also indicate a shoreward component along the Chinese and Korean coasts during both summer and winter. While the bottom velocities along the Korean coast are in agreement with bottom Ekman layer dynamics, the bottom velocities along the Zhejiang province of the Chinese coast are directed to the right of the vertically integrated velocity direction.

4. KUC and TWC Water Masses

4.1. KUC Tracer Distribution

Examination of the velocity and salinity flux fields provides some indication of the general circulation and the importance of wind forcing relative to the influence of the imposed inflow and outflow conditions. However, the velocity field and salinity fluxes do not provide a measure of the relative contributions of the KUC and TWC to the YES water masses. To aid in separating the contributions of these currents to the YES environment, tracers are added to the KUC and TWC inflow. In addition, to identify vertical movement, the tracer concentration is specified to be equal to depth. Water originating from deeper layers is identified as a tracer concentration value that is greater than the depth at which the concentration is observed.

We first examine the mean KUC tracer concentrations for summer and winter for the model experiment without wind stress (Plate 3). The areas indicated by the red contour lines in the tracer concentration plots are water mass areas determined by Liu *et al.* [1992], and the tracer concentrations are compared to these water mass areas in section 4.3. The KUC flows mainly along the shelf break (Figure 5), and the model transport boundary conditions specify that 1 Sv of the inflowing KUC exits through the Tsushima Strait (section 2). Thus the KUC is expected to be distributed along the shelf break and in the area west of Kyushu. The KUC tracer indicates additional areas of intrusion onto the continental shelf. The KUC tracer advects from the area around Cheju Island and through the Yellow Sea trough. In addition, a particularly strong intrusion occurs at 50 m in summer in the Yangtze Relict River valley.

In the no-wind model experiment the main difference between summer and winter is due to the TWC transport (section 2). At 20 and 50 m during winter, KUC concentrations increase relative to summer northeast of Taiwan and along the shelf break (Plate 3). *Hsueh et al.* [1993] and *Chern and Wang* [1992] have observed increased KUC intrusions onto the continental shelf northeast of Taiwan. Though the model indicates increased intrusion northeast of Taiwan in the tracer concentrations, the intrusions do not appear to be as strong as those observed. This may be because the observations are usually of intruding eddies and Kuroshio meander events. In the seasonal averages the amplitude of individual events is much reduced. One suggested cause for the increased winter intrusion is the increased density difference between the KUC and TWC during winter. In summer the TWC climatological inflow temperature is nearly the same as the KUC climatological inflow temperature. In winter the drop in the TWC climatological inflow temperature is much greater than the drop in the KUC climatological inflow temperature. This leads to an increased density difference between the KUC and TWC in the East China Sea. A gravity adjustment allows the KUC to flow over the TWC [*Su et al.*, 1994].

The higher summer TWC inflow provides more water mass to displace and dilute the KUC water. The low KUC concentration area in summer extending northeastward from the Taiwan Strait is due to the TWC water flowing from the Taiwan Strait to Cheju Island. The gradual KUC concentration increase from the Taiwan Strait to Cheju Island indicates the mixing of KUC water into the TWC water. The winter low TWC transport displaces and dilutes the KUC water at both depths less than during summer as evidenced by the smaller area of low KUC concentration around Cheju Island

The KUC concentration pattern with wind forcing (Plate 4) is generally similar to the concentration without wind forcing (Plate 3). One important wind stress effect is the increased winter KUC concentration northwest of Cheju Island at 20 m. This effect is related to the changes in YSWC circulation

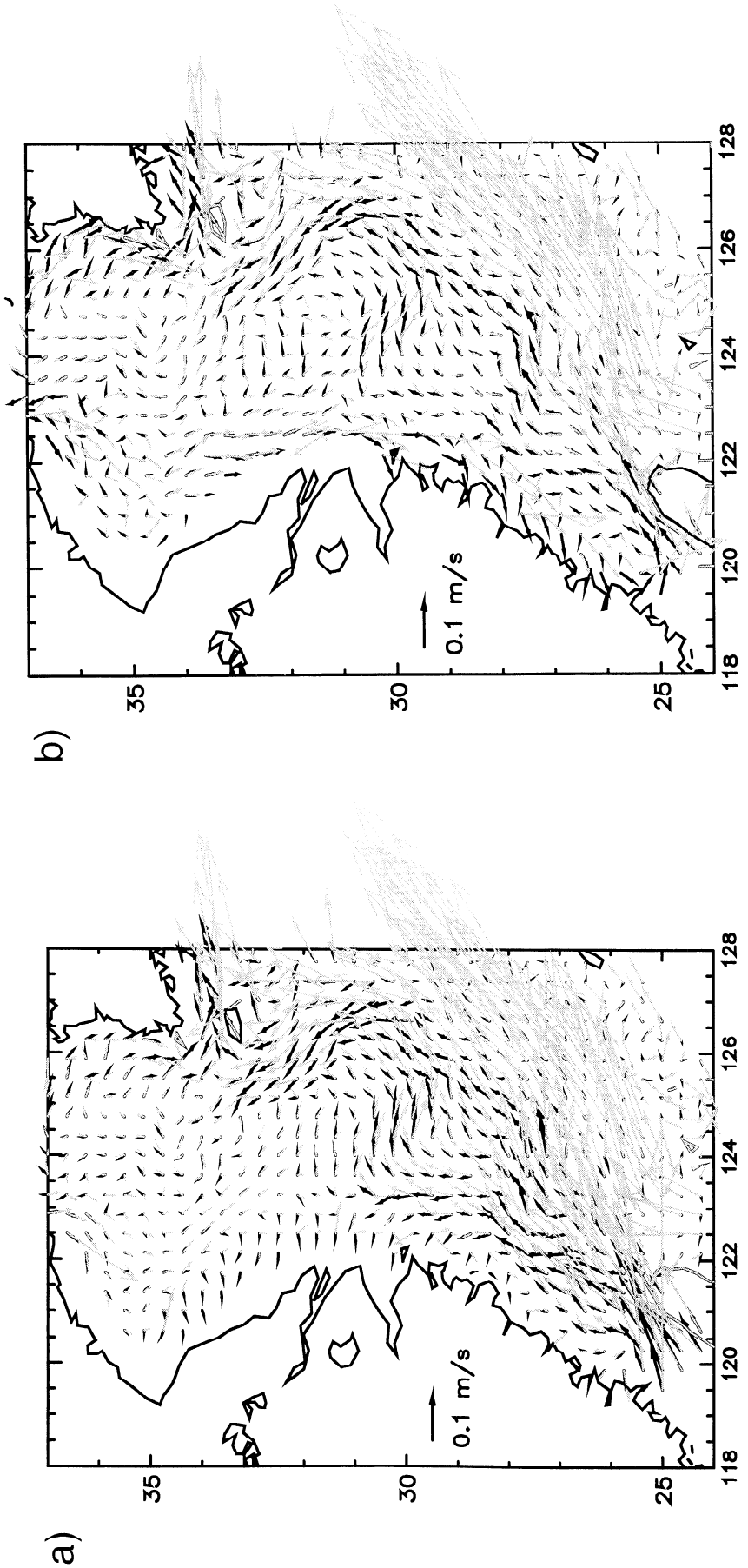

Figure 7. (a) the summer velocity and (b) the winter velocity integrated over the bottom 5 m (solid) and the velocity integrated over the water column (shaded) indicate that the bottom velocity is generally turned to the left of the total velocity. This leftward turning is a consequence of the bottom Ekman layer. The strong Taiwan Warm Current during summer generates a northward transport into the Yangtze Relict River valley that causes the summer Kuroshio upwelling. The Tsushima Current is likewise driven into the Yellow Sea by the bottom Ekman layer.

examined in section 3. The northerly winter wind stress produces an upwind current that increases the KUC concentration in the Yellow Sea. The TWC has less effect on masking the KUC intrusion into the Yellow Sea trough with wind stress. In the without-wind experiment the TWC causes the KUC concentrations to contain a minimum from the Taiwan Strait to the Cheju Island (Plate 3), whereas with the wind stress, at 20 m the KUC concentration minimum in summer extends only half the distance from the Taiwan Strait, and in winter the minimum extends less distance and is displaced toward the Chinese coast.

The reduced TWC masking with wind stress is partially due to the general smoothing of the spatial tracer patterns. The wind forcing consists of many short time period events [*Jacobs et al.*, 1998a], and these events cause short time period advection of the tracers. The resulting seasonally averaged concentrations are then smoother. To demonstrate this, we examine the temporal tracer concentration variations along one of three transects (Figure 8). The transects are lettered A, northeast of Taiwan near the KUC and TWC inflow (Figure 9); B, extending into the Yangtze Relict River valley (Figure 10); and C, over the Yellow Sea trough just west of Cheju Island extending to the Shandong peninsula (Figure 11). Concentrations at both 20 and 50 m are examined at each transect.

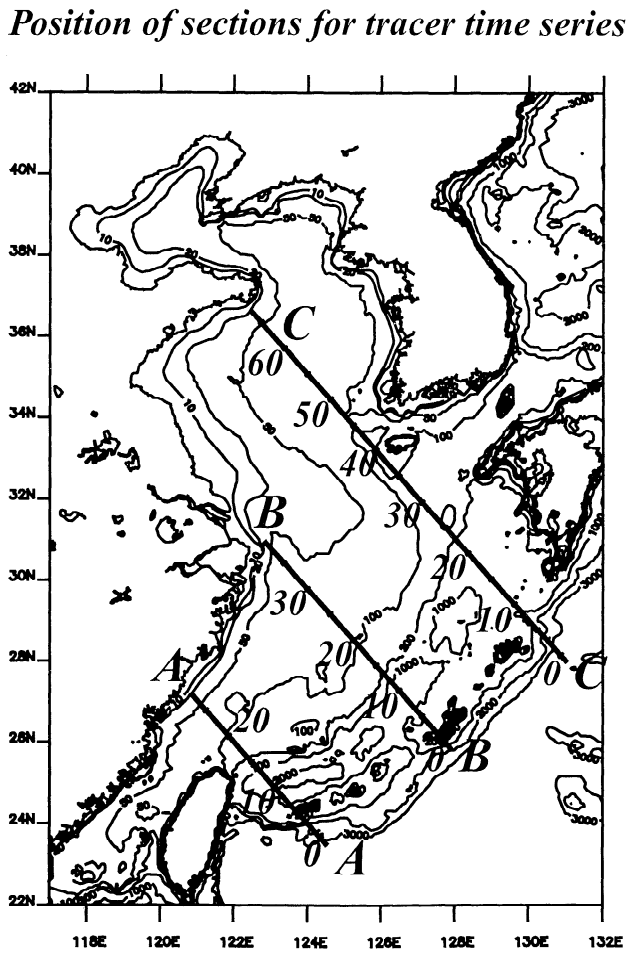

Figure 8. The three transects across which the concentrations are examined cover the inflow of the Kuroshio and Taiwan Warm Current, the Yangtze Relict River valley, and the Yellow Sea trough.

The inflow at transect A (Figure 9) demonstrates the wind-driven short time period horizontal advection of the KUC and TWC waters. The shelf break, between 100 and 200 m depth, is between points 16 and 21 along transect A. Without wind stress the boundary between the KUC and TWC waters is relatively well defined at point 19 with the KUC to the south and the TWC to the north. The short time period movements of each water are of relatively low concentration and do not extend far into the area covered by the other water. The intrusions are due to flow instabilities such as eddies and current meanders. Between points 15 and 20, several high concentration KUC intrusions occur during winter. These may be the eddy and Kuroshio intrusions as observed by *Hsueh et al.* [1993] and *Chern and Wang* [1992] that are not apparent in the seasonally averaged tracer concentrations. In the model experiment with surface wind stress, there are short events with periods of 1 week or less. These events contain water movements of higher concentration and further extent than the case without wind stress. The short time period movements create the smoother spatial distribution in the seasonal averages.

4.2. TWC Tracer Distribution

The TWC concentration without wind stress (Plate 5) indicates the TWC flowing mainly from the Taiwan Strait to the Tsushima Strait. Concentrations are much higher in the summer because of the increased inflow of TWC water. The increased total TWC water mass during summer does not dilute as readily as the smaller amount of winter TWC water. The TWC concentration along transect A (Figure 9) indicates the increased TWC flow during the spring and summer. TWC concentrations gradually decrease as the TWC flows across the East China Sea, suggesting that the TWC water mixes with the surrounding water (Plate 5). One additional mechanism allowing farther TWC penetration into the East China Sea during summer is the increased TWC velocity. This allows less horizontal diffusion as the water advects across the continental shelf in less time.

As in the case of the KUC tracer, with the wind stress the TWC tracer concentrations generally decrease (Plate 6). The summer TWC distribution is similar between the with- and without-wind stress experiments since the summer southeasterly monsoon winds are generally weak and have little affect on circulation. In winter the TWC peak concentration decreases, and the tracer extends farther northward into the Yellow Sea than in the case without wind stress.

4.3. Comparison to Water Mass Distributions

Tracer distributions are compared to the water mass results of *Liu et al.* [1992] (hereinafter referred to as L92), who use a fuzzy cluster analysis of historical in situ temperature and salinity data to delineate areas of differing water masses at the surface and at the bottom in the YES area. In the tracer concentration plots (Plates 3-6) we overlay the water mass areas of the Kuroshio water mass (southernmost area); the Taiwan Warm Current water mass in the Taiwan Strait; the East China Sea water mass, which is directly north of the Kuroshio water mass; the Yellow Sea water mass (northernmost area); and the mixed water mass lying between the East China Sea and Yellow Sea water masses. The area distribution of each water mass changes seasonally and is different at the surface and bottom. One significant difference between the analysis here and that of L92 is that we present our results at 20 and 50 m, while the in situ results are derived at the surface and bottom. The tracer

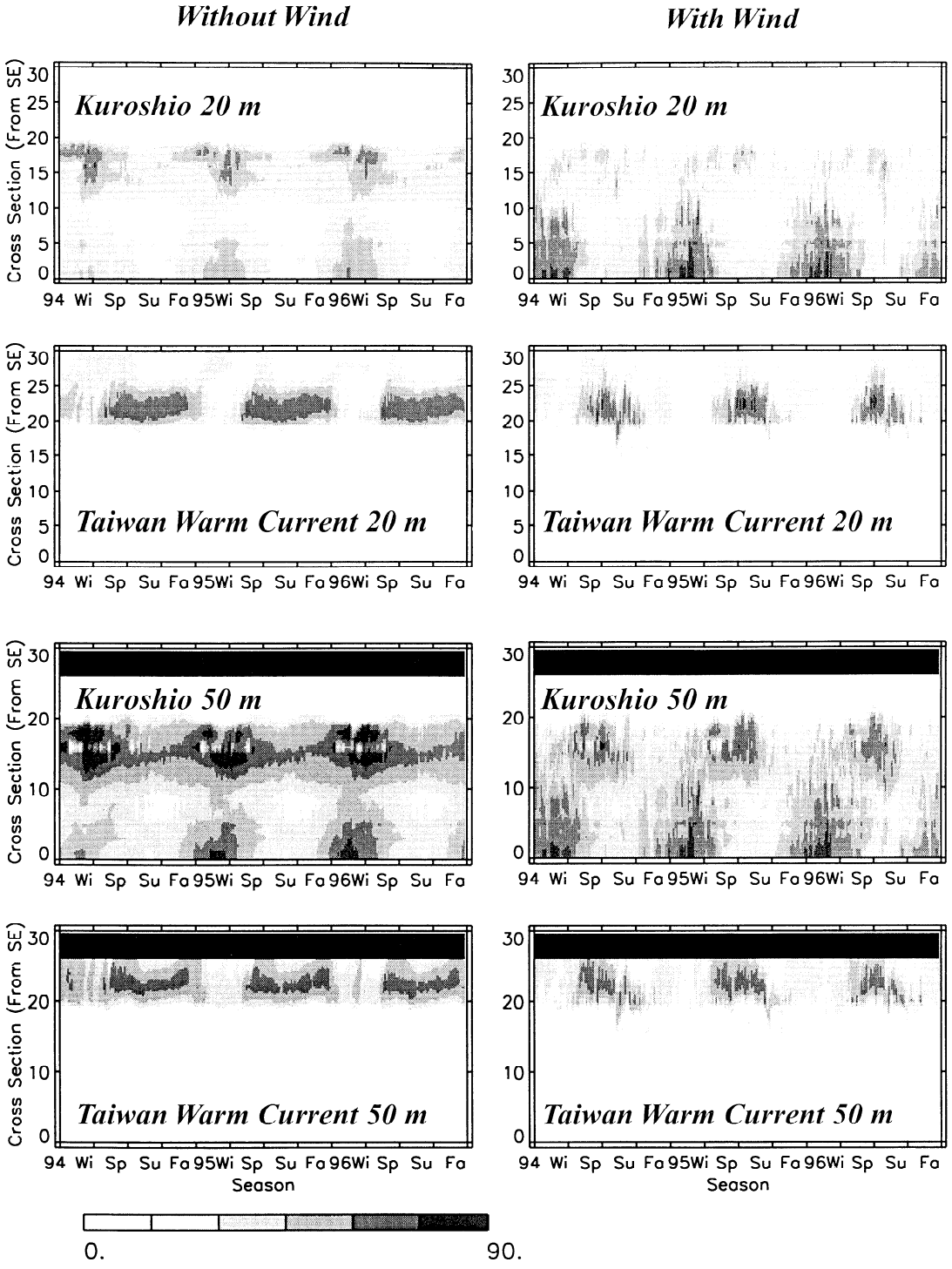

Figure 9. The Kuroshio and Taiwan Warm Current tracer concentrations along transect A indicate seasonal variations due to the Taiwan Warm Current transport. Including wind stress forces short time period and spatially extensive intrusions of the waters into one another.

distribution comparison to the water mass areas provides an indication of the contribution of the KUC and TWC to the water masses. Similar water mass analysis results are presented by *Hur et al.* [1999] using a cluster analysis of 40 years of National Ocean Data Center hydrographic data. *Su and Weng* [1994] provide a cluster analysis using two years of hydrographic data in the Yellow Sea, which also provides similar results.

The tracer distributions with wind stress applied to the model (Plates 4 and 6) indicate the origins or contributors to the main water masses. Comparison of the 20 m concentrations with the surface water mass distribution of L92 is the clearest. The KUC is generally the sole contributor to the surface Kuroshio water mass (southernmost area), with only small contributions from the TWC. This is evident as the TWC concentration is near 0 in

the Kuroshio water mass area. The surface East China Sea water mass of L92 is directly north of the Kuroshio water mass. The KUC and TWC each make different contributions to the East China Sea water that depend on season and position. Generally, the TWC makes the largest contribution to the surface East China Sea water mass. The KUC intrudes into the surface East China Sea water mass area along its southern boundary. Thus the surface East China Sea water mass is a mixture of the KUC and TWC water masses.

The surface Yellow Sea water mass (northernmost area in Plates 4 and 6) strongly depends on season. The expanded area covered by the water mass in summer is due to warming that produces near-uniform surface temperatures. During winter, water masses are differentiated more by salinity. The analysis of

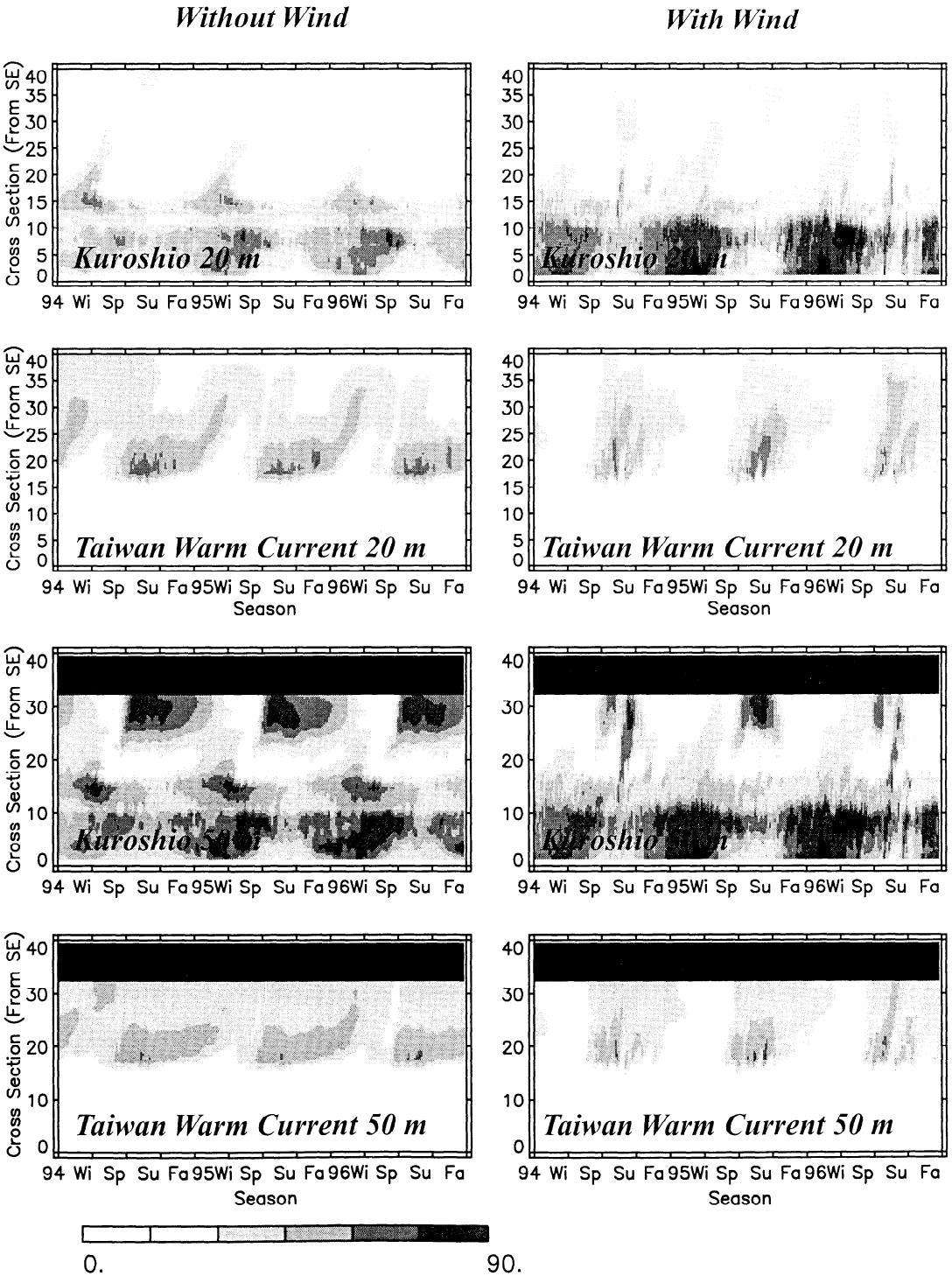

Figure 10. The Kuroshio and Taiwan Warm Current tracer concentrations along transect B indicate the Kuroshio intrusion into the Yangtze Relict River valley. The wind stress decreases the temporal extent over which the Kuroshio intrudes.

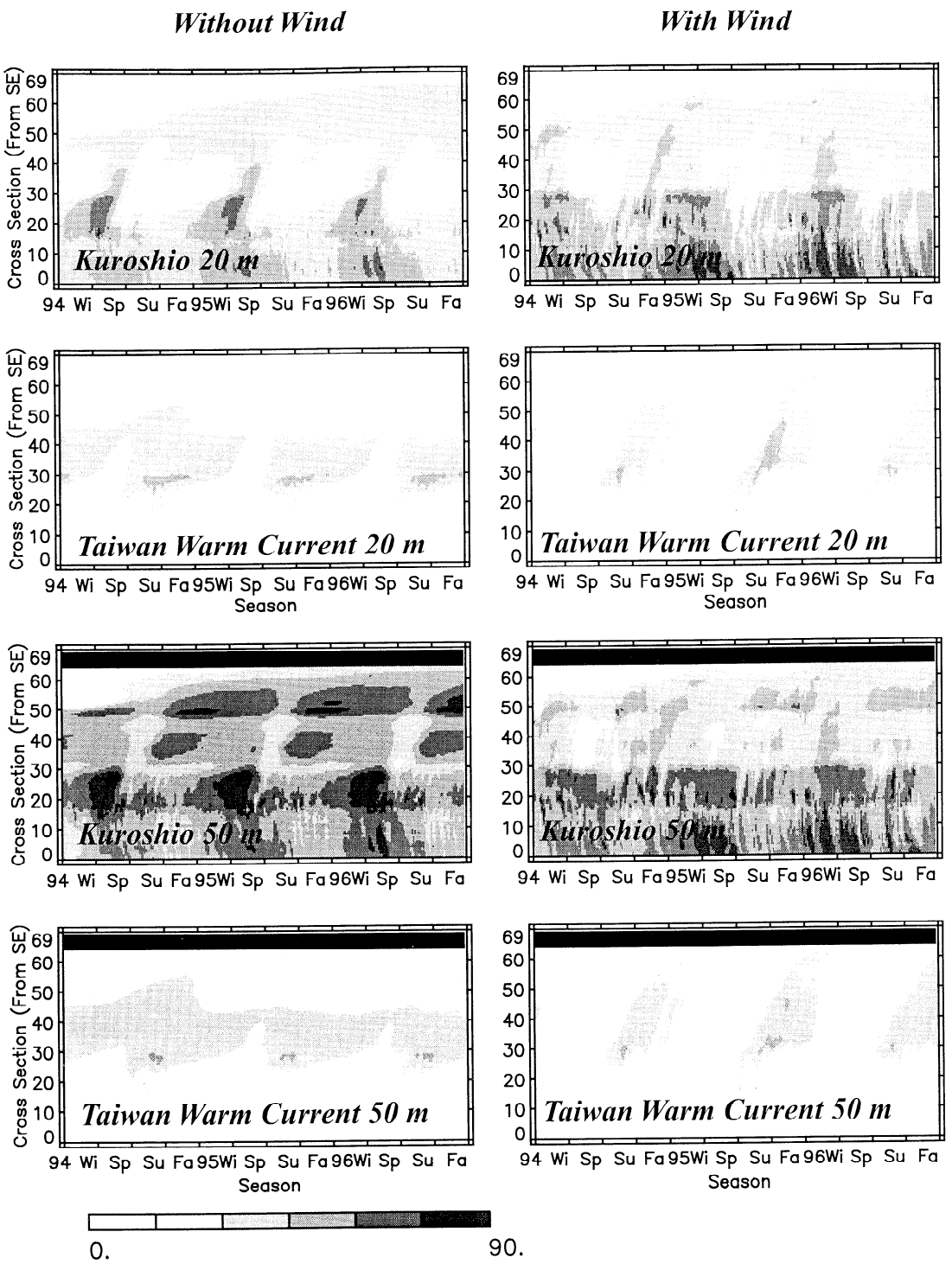

Figure 11. The Kuroshio and Taiwan Warm Current tracer concentrations along transect C indicate the Kuroshio intrusion into the Yellow Sea trough. Without wind stress the Kuroshio intrudes into the Yellow Sea trough (north of point 40) while the Taiwan Warm Current does not. With wind stress the fall and winter Kuroshio intrudes further, and the Taiwan Warm Current intrudes into the Yellow Sea.

Hur et al. [1999] delineates the separation of Yellow Sea, East China Sea, and mixed water masses most distinctly during winter. Thus the summer surface water mass areas are not as indicative of their origins as the winter water mass areas. Both the KUC and TWC contribute to the winter Yellow Sea and mixed water masses. Cluster analyses such as that of *Hur et al.* [1999] indicate that the mixed water mass lies between the Kuroshio Water and Yellow Sea Water in temperature-salinity space. The winter surface mixed water mass indicates a northward intrusion along the Yellow Sea trough that covers the area of a high-concentration KUC water intrusion (Plate 4). Comparison of the surface winter mixed water mass area with

the TWC tracer (Plate 6) indicates northward movement of TWC water across the entire boundary from the East China Sea area to the mixed water mass area.

Comparison of the 50 m concentrations to the bottom water mass areas from L92 is more difficult. The largest discrepancy in comparison is the summer TWC concentration at 50 m, which is high in the Kuroshio water mass area (Plate 6). This is due to L92's examining the bottom water and our examining the water at 50 m. As discussed previously, the bottom friction layer produces a northward transport of Kuroshio water beneath the TWC into the Yangtze Relict River valley, particularly during summer (Plate 4). The broad summer bottom Kuroshio water mass area of L92 indicates the intrusion of Kuroshio water into the Yangtze Relict River valley where the high KUC tracer concentration appears.

5. Discussion

The numerical model certainly has several unrealistic components, and these must be kept in mind while examining the results. One large deviation from true physics is the artificially closed boundary to the southeast. Since no transport occurs through this boundary, the KUC may not lose tracer concentration to the open ocean. This implies that the KUC concentrations may be biased high. Also, the closed southeastern boundary excludes transport due to the Kuroshio recirculation gyres. The recirculation gyres cause the Kuroshio transport through the Tokara Strait south of Kyushu to be much higher than the transport off Taiwan. With a closed boundary the recirculation transport is not included.

The specified boundary conditions certainly contain errors and induce errors indirectly. The Chinese Coastal Current is a combination of wind forcing and a mass balance due to the northward YSWC flow. The Chinese Coastal Current normally flows southward, with a portion passing through the Taiwan Strait close to the Chinese coast. With the specified Taiwan Strait velocity the Chinese Coastal Current in the Taiwan Strait is forced to turn to the northeast and join the TWC. Thus, although the TWC transport is specified in the strait, the transport on the shelf may be overestimated because of this effect. Since the bottom Ekman transport is related to the transport far from the bottom, the KUC upwelling in the Yangtze Relict River valley may be overestimated. However, when the TWC transport is largest in summer, the wind stress is generally southerly, and the Chinese Coastal Current transport south of the Yangtze River mouth is small. Thus the summer TWC transport across the shelf is not expected to be significantly impacted by this effect. Examination of the spring KUC tracer concentration also indicates upwelling in the Yangtze Relict River valley and at this time the TWC transport is 1.3 Sv, which is just over half the summer's 2.5 Sv.

The model experiment results indicate northward movement of KUC waters into the Yellow Sea in two principle shelf areas. The first is at the Yangtze Relict River valley, and the second is at the Yellow Sea trough. The TWC also indicates northward intrusions in these same areas. We examine the temporal concentration variations across transects B and C through these areas (Figure 8).

5.1. Yangtze Relict River Valley Intrusions

The summer mean without-wind KUC spatial distribution (Plate 3) indicates an upwelling in the Yangtze Relict River valley at 50 m through a tracer concentration greater than the water depth. A low KUC concentration area separates the Yangtze Relict River valley from the shelf break, and this area is caused by the TWC flow through the region (Plate 5). The situation is also visible in the tracer concentration transect B (Figure 10) where high concentration KUC water appears north of the TWC during summer. The high KUC concentration appears regardless of the wind forcing. In addition, the KUC concentration with wind forcing is diminished, indicating that the wind stress is not the mechanism for transporting the KUC water northward.

Along transect B (Figure 10) the TWC remains north of the 100 m isobath (at point 18), the main portion of the KUC is south of the 100 m isobat, and the Yangtze Relict River valley is north of point 25. Transect B indicates many of the features observed in transect A, namely, the increased short time period intrusions of the KUC and TWC into one another with wind stress and the decreased KUC concentration during high TWC transport.

Without wind stress the northward transport of KUC water into the Yangtze Relict River valley near the bottom is observed in the KUC concentration at 50 m depth extending from summer through winter. The peak concentration of this water indicates that the water originates from a depth of at least 75m. At 20 m, a northward transport of higher concentration KUC water occurs from the shelf break during winter. The northward movement of this water begins at the time when the TWC is weakest. The northward 20 m KUC intrusions do not have a local minimum separating the areas north and south of the shelf because the TWC flow is weak. A northward movement of the TWC slightly precedes the northward movement of the KUC in winter.

With wind stress included, at 50 m the KUC high concentration in the Yangtze Relict River valley (north of point 25) is restricted to a much shorter time. Instead of extending from summer through winter as in the without-wind experiment, the 50 m KUC high concentration occurs mainly in summer. The wind-driven circulation produces a southward flow (Figure 6) that reduces the northward KUC intrusion.

The KUC Yangtze Relict River valley concentration is highest in summer. From the standpoint of the bottom Ekman layer this situation occurs because of the increased TWC velocity across the East China Sea in summer. The stronger summer TWC generates higher transports in the bottom Ekman layer. The propensity for subsurface KUC intrusions during the summer due to the warmer and thus less dense shelf waters [*Su et al.*, 1994] may also aid in spreading the KUC water across the bottom of the East China Sea shelf.

Hu [1994] examines the upwelling along the Zhejiang province south of the Yangtze River mouth. By comparison with vertical current measurements the local wind stress is shown to be an order of magnitude weaker than that required to produce the observed upwelling. In fact, bottom currents are observed shoreward in winter with northeasterly wind. *Hu* [1994] suggests that the upwelling is supported by the bottom Ekman layer that transports water to the China coast. Observed transport direction near the bottom is directed shoreward in agreement with the bottom-averaged currents from the model experiments (Figures 7a and 7b). The model experiments indicate a narrow southward current directly offshore the Chinese coast and bottom currents oriented to the right of the average velocity. Thus the Chinese coast upwelling is possibly an extension of the northward transport across the shelf from the Yangtze Relict River valley.

Another view of the KUC intrusions through the bottom boundary layer is provided by a vertical section along transect B (Plate 7). The summer-averaged KUC tracer concentrations along the continental slope, along the shelf break, and along the continental shelf are greater than the water depth. To observe this more clearly, the tracer concentration is divided by depth, and we refer to the concentration divided by depth as the normalized concentration. Normalized concentration values >1 indicate water that has moved up from deeper areas. The KUC concentration on the bottom of the continental shelf has originated from deeper water. Thus the bottom boundary layer appears to pull the KUC water onto the continental shelf, where the water is then pushed upslope toward the Chinese coast. We refer to this process as the intrusion of the KUC into the Yangtze Relict River Valley, though a term such as the pumping of the KUC into the Yangtze Relict River Valley may provide a more correct sense of the physical mechanism.

The isoconcentration lines within the TWC (Plate 7) also indicate the up-slope movement in the bottom boundary layer. The bottom boundary layer thickness is ~30 m. The surface boundary layer may be identified in the tracer concentrations as the area where isoconcentrations are near vertical. For example, the TWC tracer concentration between points 10 and 15 indicates a mixed layer depth >50 m. The surface and bottom layers appear to meet at 50 m near point 34. The very large normalized concentrations from the surface to ~15 m are a result of the surface mixed layer. The tracer concentration at the base of the mixed layer is mixed vertically to the surface. Concentrations values near the surface are divided by small depth values, and this leads to the high normalized surface concentrations.

The results here indicate that the Kuroshio is continually intruding onto the shelf, with surface intrusion during winter and bottom intrusion during summer (Figure 10). *Su et al.* [1994] suggests that this process is the result of the seasonal variations in shelf water density. As the shelf waters cool in the fall and winter, the less dense KUC water intrudes northward through the surface, overriding the denser shelf water. During summer the situation is reversed. The denser KUC water intrudes beneath the warm, less dense shelf water. In addition to these density variations, the bottom boundary layer appears to be a contributing factor.

Previous CTD studies have found intrusions of the KUC onto the continental shelf northeast of Taiwan [*Liu et al.*, 1992]. Additional surveys have found evidence of KUC water spread across wide areas of the bottom of the East China Sea. *Su et al.* [1994] examine historical hydrographic data at the TWC inflow to the East China Sea and find that the bottom shelf is covered

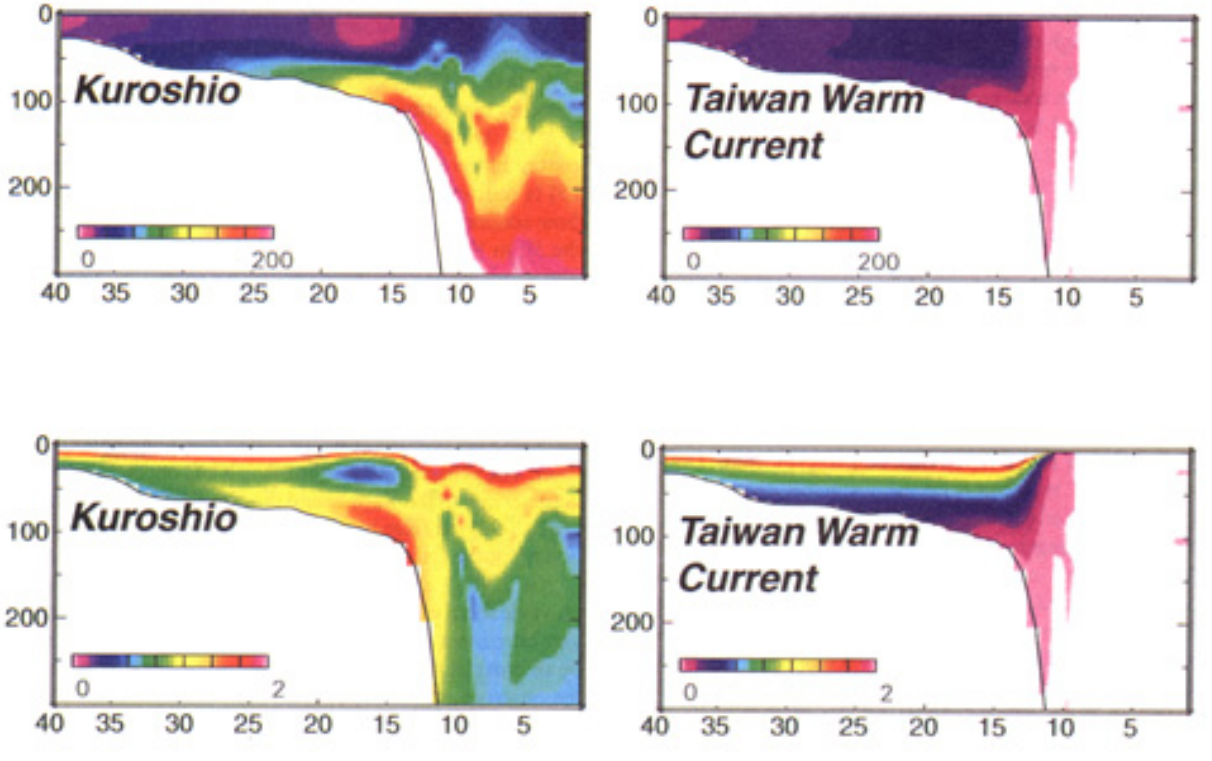

Plate 7. The summer averaged KUC tracer concentration (top left) and TWC tracer concentration (top right) along transect B indicate the deep KUC water intruding onto the continental shelf beneath the TWC. The TWC concentration isolines are pushed towards the shallower water within the bottom boundary layer. The tracer concentration boundary conditions specify the concentration as equal to the depth. To show where upwelled waters exist, the concentration is divided by depth. The KUC normalized concentration (bottom left) indicates the waters along the continental slope, shelf break, and up continental shelf are upwelled (concentration is greater than the depth, or normalized concentration is greater than 1). The high normalized concentrations near the surface in both the KUC and TWC are due to surface mixed layer bringing concentrations from near the base of the mixed layer to the surface where the concentration is then divided by the small depth.

by Kuroshio subsurface water during summer. *Guan* [1994] indicates that the bottom water in the southwest East China Sea has a tendency of "upclimbing" and "coast-approaching." Additional works note that the KUC intrusions provide the bottom portion of East China Sea Water [*Weng and Wang*, 1984; *Su and Pan*, 1987; *Su et al.*, 1990].

5.2. Yellow Sea Warm Current Intrusion

Transect C (Figure 11) is placed to examine the TSC and YSWC flow variations into the Yellow Sea. The shelf break near point 25 indicates a division between the flow on and off the continental shelf. Some long-period trends do appear in the 20 m KUC concentration without wind stress. The area covered by the KUC concentration north of point 40 slowly increases over the 3 year model experiment. This indicates that the tracer concentrations have not completely reached a steady state. The long time period transients also indicate that changes in the KUC or TWC properties can generate a relatively slow response in the Yellow Sea environment.

The TWC concentrations are constrained mainly to the continental shelf; however, as indicated in Plates 5 and 6, small TWC concentrations do appear along the southwestern Kyushu coast. Along transect C the division between the Yellow Sea and East China Sea occurs near Cheju Island, which is near point 40. Observations have shown the TSC flowing from the KUC near the shelf break northward to the area of Cheju Island [*Lie and Cho*, 1994]. The model without wind stress indicates the TSC flow in the KUC tracer during spring at 20 m as a high concentration intrusion from the shelf break (point 25) to Cheju Island (point 40). At 50 m the KUC tracer indicates a northward penetration into the Yellow Sea during fall through spring. The 50 m KUC concentration contains a local minimum between points 25 and 35 during summer and fall. This situation is similar to that at transect B where the high TWC flow causes the displacement and diffusion of the KUC water mass. The TWC concentration indicates a maximum at the same location and during the same time as the KUC minimum.

The KUC at 50 m also indicates some upwelling in the Yellow Sea during times of strong TWC flow. During summer and fall the high KUC concentration north of point 40 may be due to northward flow along the bottom beneath the TWC.

With wind stress, higher winter KUC concentrations appear at 20 m in the Cheju Island vicinity for a longer portion of the year than without wind stress. The higher concentration is also apparent in the spatial distribution of the KUC tracer (Plates 3 and 4). There are two reasons for this effect. The main reason is the increased northward TSC transport during winter in response to the wind stress. The increased northward flow is apparent in the winter mean velocities at 20 m (Figure 6). The higher TSC flow advects the KUC tracer to Cheju Island. A secondary reason is that the wind stress causes a dilution of the TWC upstream of transect C. Without wind stress the KUC distribution generally indicates a local minimum extending from the Taiwan Strait toward Cheju Island (Plate 3). With wind stress the KUC concentration minimum does not extend as far from the Taiwan Strait (Plate 4). With wind stress the lower concentration TWC waters at transect C do not dilute the KUC as greatly as in the case without wind stress.

Previous studies have suggested the importance of wind forcing for driving subsurface KUC waters northward during winter [Park, 1986; *Hsueh*, 1988]. Evidence from the model experiments supports this, but the results also suggest that the wind stress is not necessary for the KUC water to flow into the Yellow Sea. In the model experiment without wind stress, KUC water appears in the Yellow Sea at both 20 and 50 m during winter and spring. The seasonal intrusions are due to changes in the strength of the TWC, which appear to displace or block KUC water on the shelf and thus prevent the movement of the KUC northward. However, the model experiment without wind stress shows that the TWC does not intrude seasonally into the Yellow Sea. At both 20 and 50 m the TWC indicates a slow diffusion into the Yellow Sea with little seasonal cycle north of point 40. When the wind stress is applied to the model, the TWC concentration extends much farther northward during fall. In addition, the KUC intrusions at 20 m indicate stronger and farther extension northward into the Yellow Sea when wind stress is applied.

6. Conclusions

Two model tracer experiments are used to examine the effects of TWC and KUC variations as well as wind stress on the YES environment. Separating the KUC and TWC water masses from measurement of in situ water properties is difficult because of the similarity of the two water types. The TWC flows from the South China Sea where the water properties are strongly controlled by the KUC because of KUC intrusions through the Luzon Strait. By inserting two separate tracers into the numerical model we attempt to separate and understand the influence of the TWC and KUC. The seasonal variations in transport at the Taiwan Strait and Tsushima Strait provide the influence of current variations, while two separate model experiments provide the influence of wind stress.

Results indicate that upwelled KUC water appears near the bottom on the north side of the TWC in summer. The stronger summer TWC generates a bottom Ekman layer that transports KUC water beneath the TWC. Northward moving bottom KUC water appears in the Yangtze Relict River valley, and the upwelling along the Chinese coast in the East China Sea appears to be a result of this bottom boundary layer.

Without wind stress the Chinese and Korean coastal currents are generated in response to the YSWC inflow. The winter northerly wind stress strongly reinforces the southward coastal currents, which in turn increase the northward TSC and YSWC transport. The short time period wind events cause short time period advection of the different water masses. The wind stress also results in spatial smoothing and decreased peak water mass concentrations.

Both the KUC and TWC tracers appear in the Yellow Sea year-round without wind stress. However, the appearance of the tracers does not imply year-round flow into the Yellow Sea. Without wind stress the KUC tracer flows into the Yellow Sea during winter at 20 m and during summer through winter at 50 m. The TWC does not flow significantly into the Yellow Sea without wind stress. With wind stress both the KUC and TWC flows into the Yellow Sea increase at 20 m, and the TWC flow increases at 50 m.

Acknowledgments. This work was sponsored by the Office of Naval Research (program element PE0601153N) as part of the projects "Yellow and East China Seas Response to Winds and Currents," and "Dynamical Linkage of the Asian Marginal Seas." This work is a contribution of the Naval Research Laboratory, number JA/7323-98-0068. Two anonymous reviewers took the time and effort to help us dramatically improve this manuscript; thanks!

References

Beardsley, R. C., R. Limeburner, H. Yu, and G. A. Cannon, Discharge of the Changjiang (Yantze River) into the East China Sea, *Cont. Shelf Res., 4*, 57-76, 1985.

Blumberg, A., and G. Mellor, A description of a three-dimensional coastal ocean circulation model, in *Three-Dimensional Coastal Ocean Models, Coastal Estuarine Sci.*, vol. 4, edited by N.S. Heaps, pp. 1-16, AGU, Washington, D.C., 1987.

Chen, C., R. Beardsley, R. Limeburner, and K. Kim, Comparison of winter and summer hydrographic *observations* in the Yellow Sea and East China Seas and adjacent Kuroshio during 1986, *Cont., Shelf Res., 14*, 909-929, 1994.

Chern, C. S., and J. *Wang*, The influence of Taiwan Strait waters on the circulation of the southern East China Sea, *Mer, 30*, 223-228, 1992.

Chuang, W. S., and W. D. Liang, Seasonal variability of intrusion of the Kuroshio water across the continental shelf northeast of Taiwan, *J. Oceanogr., 50*, 531-542, 1994.

Dianrong, Y, K. Buarui, Z. Yulin, and Z. Dejian, Diagnostic study of the summer thermocline depth in the Huanghai Sea and the East China Sea, *Haiyang Xuebao Zhongwenban, 9*, 331-342, 1990.

Fang, G., B. Ahao, and Y. Zhu, Water volume transport through the Taiwan Strait and the continental shelf of the East China Sea measured with current meters, in *Oceanography of Asian Marginal Seas*, edited by K. Tokano, pp. 345-358, Elsevier, New York, New York, 1991.

Guan, B. X., Patterns and structures of the currents in Bohai, Huanghai, and East China Seas, in *Oceanology of the East China Seas*, vol. 1, edited by Z. Di et al., pp. 17-26, Kluwer Acad., Norwell, Mass., 1994.

Hogan, T. F., and L. R. Brody, Sensitivity studies of the Navy global forecast model *parameterizations* and evaluation of improvements to NOGAPS, *Mon. Weather Rev., 121*, 2373-2395, 1993.

Hogan, T. F., and T. E. Rosmond, The description of the Navy Operational Global Atmospheric Prediction System, *Mon. Weather Rev.*, 119, 1786-1815, 1991.

Hsueh, Y., *Recent* current observations in the eastern Yellow Sea, *J. Geophys. Res., 93*, 6875-6884, 1988.

Hsueh, Y., C. S. Chern, and J. Wang, Blocking of the Kuroshio by the continental shelf northeast of Taiwan, *J. Geophys. Res., 98*, 12,351-12,359, 1993.

Hu, D. X., Some striking features of the circulation in Huanghai Sea and East China Sea, in *Oceanology of the East China Seas*, vol. 1, edited by Z. Di et al., pp. 27-38, Kluwer Acad., Norwell, Mass., 1994.

Hur, H. B., G. A. Jacobs, W. J. Teague, Monthly water mass analyses in the Yellow and East China Seas, *J. Oceanogr., 55*, 171-184, 1999.

Jacobs, G. A., W. J. Teague, S. K. Riedlinger, R. H. Preller, and J. P. Blaha, Sea surface height variations in the Yellow and East China Seas, 2, SSH variability in the weekly and semiweekly bands, *J. Geophys. Res., 103*, 18,479-18,496, 1998a.

Jacobs, G. A., R. H. Preller, S. K. Riedlinger, and W. J. Teague, Coastal wave generation in the Bohai Bay and propagation along the Chinese coast, *Geophys. Res. Lett., 25*, 777-780, 1998b.

Kantha, L. H., and C. A. Clayson, An improved mixed layer model for geophysical applications, *J. Geophys.* Res., *99*, 25,235-25,266, 1994.

Katoh, O., K. Teshima, C. Abe, H. Fujita, K. Miyaji, K. Morinaga, and N. Nakagawa, Process of the Tsushima Current formation revealed by ADCP measurements in summer, *J. Oceanogr., 52*, 491-507, 1996.

Lie, H. J., Summertime hydrographic features in the southeastern Hwanghae, *Prog. Oceanogr.*, 17, 229-242, 1986.

Lie, H. J., and C. H. Cho, On the origin of the Tsushima Warm Current, *J. Geophys. Res.*, 99, 25,081-25,091, 1994.

Lie, H. J., C. H. Cho, J. H. Lee, P. Niiler, and J. H. Hu, Separation of the Kuroshio water and its penetration onto the continental shelf west of Kyushu, *J. Geophys. Res., 103*, 2963-2976, 1998.

Liu, K. K., G. C. Gong, C. Z. Shyu, S. C. Pai, C. L. Wei, and S. Y. Chao, Response of Kuroshio upwelling to the onset of the northeast monsoon in the sea north of Taiwan: Observations and a numerical simulation, *J. Geophys. Res.*, 97, 12,511-12,526, 1992.

Liu, S., X. Shen, W. Youqin, and H. Shixin, Preliminary analysis of distribution and variation of perennial monthly mean water masses in the Bohai Sea, the Huanghai Sea, and the East China Sea, *Haiyang Xuebao Zhongwenban, 11*, 483-498, 1992.

Nitani, H., Beginning of the Kuroshio, in *The Kuroshio,* edited by H. Stommel and K. Yoshida, pp. 129-163, Univ. of Wash. Press, Seattle, 1972.

Park, Y-H, Water characteristics and movements of the Yellow Sea Warm Current in summer, *Prog.* Oceanogr. *17*, 243-17,254, 1986.

Qiu, B., and N. Imasato, A numerical study on the formation of the Kuroshio Counter Current and the Kuroshio Branch Current in the East China Seas, *Cont. Shelf Res., 10*, 165-184, 1990.

Rosmond, T. E., The design and testing of the Navy Operational Global Atmospheric Prediction System, *Weather Forecasting, 7*, 262-272, 1992.

Su, J. L., and Y. Q. Pan, On the shelf circulation of the Kuroshio north of Taiwan, *Haiyang* Xuebao *Zhongwenban, 6*, suppl. I, 1-20, 1987.

Su, J. L, B. X. Guan, and J. Z. Jiang, The Kuroshio, part I, Physical features, *Oceanogr. Mar.* Biol., *28*, 11-71, 1990.

Su, J. L, Y. Q. Pan, and X. S. Liang, Kuroshio intrusion and Taiwan Warm Current, in *Oceanology of the East China Seas*, vol. 1, edited by Z. Di et al., pp. 59-70, Kluwer Acad., Norwell, Mass., 1994.

Su, Y. S., and X. C. Weng, Water masses in China Seas, in *Oceanology of the East China Seas*, vol. 1, edited by Z. Di et al., pp. 3-16, Kluwer Acad., Norwell, Mass., 1994.

Wan, B., B. Guo, and Z. Chen, A three-layer model for the thermal structure in the Huanghai Sea, *Haiyang Xuebao* Zhongwenban, *9*, 159-179, 1990.

Weng, X. C., and C. M. Wang, A preliminary study of the *T-S* characteristics and origin of Taiwan Warm Current in summer, *Stud. Mar. Sinica, 21*, 113-133, 1984.

Yang, D., G. Kuong, Y. Zhou, and Z. Dejian, Diagnostic study of the summer thrmocline depth in the Huanghai Sea and the East China Sea, *Haiyang Xuebao Zhongwenban, 9*, 331-342, 1990.

Zhao, B., Basic characteristics and forming mechanism of the sharp thermocline in the Bohai Sea, Huanghai Sea, and northern East China Sea, *Haiyang Xuebao Zhongwenban, 8*, 497-510, 1989.

Zhao, B., and G. Fang, Estimation of water volume transports through the main straits of the East China Sea, *Haiyang Xuebao Zhongwenban, 10*, 1-13, 1991.

Zheng, Q., and V. Klemas, Determination of winter temperature patterns, fronts, and surface currents in the Yellow Sea and East China Sea from satellite imagery, *Remote Sens. Environ., 12*, 201-218, 1982.

Zheng, Y., and W. Huang, A preliminary analaysis on the characteristics of the Kuroshio frontal eddy in the East China Sea in spring, *Chin. J. Oceanol. Limnol., 11*, 276-284, 1993.

H. B. Hur, Chungnam Nonsansi Dumamyun, Namsunri Military Apt., 202-402, Seoul, Korea.

G. A. Jacobs and S. K. Riedlinger, Naval Research Laboratory, Stennis Space Center, MS 39529. (jacobs@nrlssc.navy.mil; riedlinger@nrlssc.navy.mil).

(Received January 22, 1999; revised December 14, 1999; accepted April 19, 2000.)